Supplementary Information for

A Unique Bipartite Polycomb Signature Regulates Stimulus-Response Transcription during Development

Taro Kitazawa,[1,5] Dania Machlab,[1,2,3,5] Onkar Joshi,[1] Nicola Maiorano,[1] Hubertus Kohler,[1] Sebastien Ducret,[1] Sandra Kessler,[1] Henrik Gezelius,[4,6] Charlotte Soneson,[1,2] Panagiotis Papasaikas,[1,2] Guillermina López-Bendito,[4] Michael B. Stadler,[1,2] and Filippo M. Rijli[1,3*]

[*] Correspondence to: filippo.rijli@fmi.ch

[5]These authors contributed equally to this work

This PDF file includes:

Supplementary Note

Identification of activity-regulated genes in barrelette neurons

To identify activity-regulated IEGs and LRGs in developing barrelette neurons, we set out a genetic strategy to isolate E10.5 mitotic progenitors and postmitotic barrelette neurons at E14.5 (early postmitotic), E18.5 (perinatal) and P4 (consolidated barrelette stage) by fluorescence activated cell sorting (FACS) (Fig. 1a, Extended Data Fig. 1a-e, Supplementary Figs 1 and 2, Methods). For easier reference, we have identified each mouse genotype with specific abbreviations and summarized all relevant details in Supplementary Table 1. Briefly, E10.5 tdTomato^{+} mitotic progenitors were obtained by crossing the *Krox20::Cre* mouse line, which labels rhombomere 3 (r3) derivatives including ventral principal trigeminal nucleus (vPrV) barrelette progenitors[1], with the Cre-dependent $R26^{tdTomato}$ floxed reporter line ($K20^{tdTomato/+}$) (Supplementary Table 1, Supplementary Fig. 1). Postmitotic vPrV barrelette neurons were FACS-isolated by an intersectional genetic strategy. Briefly, the postmitotic *Drg11::Cre*[2] line crossed with the Cre-dependent $R26R^{ZsGreen}$ line to generate $Drg11^{ZsGreen/+}$ line (Supplementary Table 1), labeling both the lower jaw-innervated dorsal PrV (dPrV) and whisker-associated vPrV barrelette neurons[2]. $Drg11^{ZsGreen/+}$ mice were further crossed with the *r2::mCherry* ($r2^{mCherry/+}$) transgenic line[2], expressing mCherry in r2 derivatives including dPrV neurons (yellow). We then selectively sorted ZsGreen^{+} (green) vPrV barrelette neurons ($Drg11^{vPrV\text{-}ZsGreen+}$) (Supplementary Table 1; Extended Data Fig. 1c; Methods; Supplementary Fig. 2).

To achieve genetic silencing of neuronal activity in vPrV barrelette neurons, we crossed the Cre-inducible $R26^{Kir\text{-}mCherry}$ line (*Kir*)[3], conditionally overexpressing the Kir2.1 inward rectifier potassium channel fused to mCherry, with either *Krox20::Cre* ($K20^{Kir/+}$) or *Drg11::Cre* ($Drg11^{Kir/+}$) lines (Supplementary Table 1). Genetic silencing of barrelette neuron activity resulted in vPrV of normal size (Extended Data Fig. 1f) but lacking whisker-related barrelette neuron map representation by CO staining (Extended Data Fig. 1g,h), due to asymmetric dendritic tree organization of vPrV barrelette neurons (Extended Data Fig.1i-p, see Supplementary Methods), resembling the phenotype induced by whisker sensory deprivation[4-7]. To obtain mRNA-seq (Smart-seq2) profile of perinatal (E18.5) activity-deprived barrelette neurons, we collected E18.5 Kir-overexpressing postmitotic barrelette neurons ($Drg11^{vPrV\text{-}Kir/+}$), by mating $Drg11^{Kir/+}$ mice and

the *r2::EGFP* (*r2*$^{EGFP/+}$) line and selectively FACS sorting mCherry^{+} neurons (red) (Extended Data Fig. 1e; Supplementary Table 1; Methods; Supplementary Fig. 2).

Next, to identify the activity response genes (ARGs) induced in barrelette neurons at the beginning of the sensory-dependent maturation period (that spans E18.5-P2/3)[8], we compared mRNA-seq profile of FACS-sorted E18.5 activity-deprived *Drg11*$^{vPrV\text{-}Kir/+}$ barrelette neurons to those of E14.5 and E18.5 wild-type barrelette neurons. Among the genes with undetectable or low basal expression level (reads per kilobase per million mapped reads, RPKM < 3) in E14.5 barrelette neurons, we identified those genes (*n*=56) that were up-regulated at E18.5 compared with E14.5, and down-regulated in E18.5 Kir-overexpressing, activity-silenced, barrelette neurons as compared to E18.5 wild-type neurons (Extended Data Fig. 1q-s; Methods). We referred to these genes as barrelette sensory ARGs (bsARGs) (Supplementary Table 2). bsARGs comprised 4 IEGs, namely *Fos, Egr1, Junb,* and *Zfp36* (Fig. 1b and Supplementary Table 2), as well as at least 23 putative LRGs involved in calcium signaling and late aspects of activity-dependent neuronal development (e.g. *Cd38, Osmr*) (Supplementary Table 3), thus validating our strategy.

We then identified additional activity regulated genes (ARGs) (*n*=83) that were transcriptionally induced by distinct activity-dependent stimuli in neuronal types other than barrelette neurons[9-11] but that displayed undetectable or low basal expression level (RPKM < 3) in E14.5, E18.5 and P4 barrelette neurons. We referred to these genes as non-barrelette ARGs (nbARGs, see Methods). nbARGs included both LRGs and 12 IEGs that were induced, respectively, in: i) KCl-treated mouse cultured cortical neurons[10], ii) primary somatosensory (S1) barrel cortex neurons after environmental enrichment[11], and iii) light-stimulated primary visual cortex (V1) neurons[9].

The H3K27ac and H3K27me3 histone marks coexist at the promoter and gene body of bipartite genes

To establish whether the H3K27ac and H3K27me3 marks indeed coexist at the promoter and gene body of bipartite genes, respectively, we next carried out sequential ChIP-seq. Since collecting sufficient numbers of E14.5 barrelette neurons for sequential ChIP-seq and other specific chromatin experiments requiring higher cell numbers was technically challenging, we have used developmentally matched bulk hindbrain tissue (Methods); indeed, in E14.5 hindbrain tissue,

barrelette neuron E14.5Bip genes were also maintained in a bipartite state (Extended Data Figs. 3e and 4a-c).

Since the two marks are expected to be non-overlapping though covering adjacent promoter and gene body regions, we applied sequential H3K27me3 and H3K27ac ChIP-seq on 2-3kb large chromatin fragments firstly immunoprecipitated by anti-H3K27me3 and subsequently by anti-H3K27ac antibodies (Extended Data Fig. 4a; Methods). E14.5Bip genes were selectively enriched among the H3K27ac+/H3K27me3+ co-immunoprecipitated fragments (Fig. 2e, Extended Data Fig. 4b-d), demonstrating that the bipartite signature exists *in vivo* and it is not the result of allelic or cellular heterogeneity in bulk ChIP-seq data.

To further investigate the issue of cell heterogeneity and support these findings, we next carried out single-cell mRNA-seq (scRNA-seq) analysis of FACS isolated E14.5 postmitotic *Drg11*$^{vPrV\text{-}tdTomato/+}$ barrelette neurons (Supplementary Table 1, Extended Data Fig. 1d, Supplementary Fig. 2, Methods) by droplet-based encapsulation using the 10X Genomics Chromium System. We reasoned that if the H3K27ac/H3K27me3 chromatin pattern of bipartite genes is merely the result of H3K27ac or H3K27me3 heterogeneity within the bulk cell population, then, in single cells, bipartite genes (E14.5Bip) carrying only H3K27ac should express comparable levels of mRNA expression as non-bipartite (non-Bip) genes with matching H3K27ac promoter levels (E14.5AcP; Fig. 2f, left and middle, Methods). However, while the E14.5AcP genes showed detectable mRNA expression in at least 21% (mean fraction) of single cells, the E14.5Bip gene transcripts were only detected in as few as 5% of single cells (Fig. 2f, right).

In addition, scRNA-seq analysis of E10.5 *K20*$^{tdTomato/+}$ mitotic progenitors confirmed the same finding: namely, transcripts of E10.5 top 100 bipartiteness scored (E10.5Bip) genes (Supplementary Table 4) were only detected in as few as 6% of single cells, while non-Bip genes with Bip-matching H3K27ac promoter level (E10.5AcP) showed detectable expression in 30% of single cells (Extended Data Fig. 4e).

In summary, the scRNA-seq analysis together with the bulk sequential ChIP-seq data strongly support that H3K27ac/H3K27me3 coexist at the promoter/gene body of bipartite genes, correlating with low or undetectable mRNA transcription.

Visualization of mouse genes by t-SNE according to their chromatin organization in barrelette neurons

To investigate how the bipartite signature is established, maintained, and resolved during development, we created a two-dimensional (2D) projection of autosomal genes according to chromatin accessibility, H3K27me3, H3K4me2, and H3K27ac levels at promoters and gene bodies (Extended Data Fig. 5a, Methods) using t-distributed Stochastic Neighbor Embedding (t-SNE) (Fig. 3a-d, Extended Data Fig. 5b-l). We generated a single map for E10.5 progenitors (Fig. 3b) and a combined E14.5, E18.5 and P4 t-SNE map of chromatin states for postmitotic barrelette neurons (Fig. 3a, Extended Data Fig. 5b, c; Methods). Genes (i.e. dots on t-SNE plots) with similar chromatin patterns were grouped together, as illustrated by the regions of homogeneous chromatin features at promoters and gene bodies (Fig. 3a, b, Extended Data Fig. 5b, c). Gene grouping also correlated with mRNA-seq data (compare Extended Data Fig. 5c-e).

Top-scoring bipartite and bivalent genes at E10.5 and postmitotic stages mapped to distinct, largely non-overlapping, regions on the respective t-SNE maps (visualized by green and red contour lines, respectively, depicting gene densities; Fig. 3a-d; Extended Data Fig. 5f, g, k, l; Methods). At postmitotic stages, while bivalent genes were grouped, bipartite genes appeared more spatially distributed on the t-SNE, indicating varying levels of H3K27ac and H3K27me3 at the promoter and gene body. To assess this point, we focused on the E14.5Bip genes (black dots, Fig. 3a) and subdivided them into two subgroups, E14.5Bip-a (n=57) and E14.5Bip-b (n=43) genes, according to their localization on the t-SNE plot (Extended Data Fig. 5i, orange and blue dots). E14.5Bip-a genes (orange dots) carried relatively higher H3K27ac on promoter and lower H3K27me3 on gene body (Extended Data Fig. 5j, left and middle); conversely, E14.5Bip-b genes (blue dots) carried relatively lower H3K27ac on promoter and higher H3K27me3 on gene body (Extended Data Fig. 5j, left and middle). To understand whether these differences might be biologically meaningful and correlate them with distinct transcript production, we analyzed mRNA levels. Indeed, E14.5Bip-b genes (blue cluster), located on t-SNE close to the bivalent region (Extended Data Fig. 5i), produced less transcripts than Bip-a genes (Extended Data Fig. 5j, right), located farther away from E14.5Bip-b genes on the t-SNE map and closer to active genes (Extended Data Fig. 5i, orange cluster).

Furthermore, the combined E14.5-E18.5-P4 t-SNE plot permitted to visualize chromatin state changes of each bipartite gene during neuron development (Fig. 3a-d). Namely, genes mapping to the same region of the combined t-SNE map at different developmental stages would reveal a stable chromatin state, whereas genes changing their localization between developmental

stages change their chromatin state (see Fig. 3c,d). Note that the three stages are homogenously mixed on the combined t-SNE (Extended Data Fig. 5b), indicating that gene clustering was conducted without potential stage-specific bias. To illustrate the dynamic nature of bipartite genes, we plotted on a t-SNE map all genes colored according to their overall change of chromatin state between E14.5 and P4 (Extended Data Fig. 5h, Methods). This analysis confirmed that bivalent genes tend to be more stable compared with bipartite genes and revealed that bipartite genes are the most dynamic of all genes, in terms of chromatin state change, during development.

The bipartite signature at the *Fos* locus allows for active enhancer-promoter contacts irrespective of productive transcription

Developmental analysis of the *Fos* locus revealed additional features of the bipartite chromatin organization (Fig. 3e). The *Fos* locus contains five activity-regulated enhancers (e1-e5) combinatorially activated in a stimulus-dependent manner in cultured and *in vivo* neurons[12-14]. In E10.5 progenitors and E14.5 early postmitotic neurons, even though *Fos* mRNA was barely detected, its promoter, e2, e5 and also e1 displayed active histone marks. At E18.5, phosphorylated CREB (pCREB), a readout of stimulus-dependent transcription[15], increased at the promoter and *Fos* was transcriptionally induced; the gene body was almost devoid of H3K27me3 and partially switched to H3K27ac. At P4, productive transcription and pCREB levels at the *Fos* promoter and e2 and e5 enhancers were further increased (Fig. 3e).

Circularized Chromosome Conformation Capture sequencing (4C-seq) of E10.5, E14.5, E18.5, and P4 bulk hindbrain tissue (Methods) using the *Fos* promoter, e2, and e5 as viewpoints revealed reciprocal physical interactions during development (Extended Data Fig. 6c), showing that the active promoter interacts with active enhancers, irrespective of net productive transcriptional output. On the other hand, enhancer acetylation levels change during development (Fig. 3e) as well as the frequencies of specific enhancer-promoter interactions in response to different stimuli[12].

Additional chromatin features of bipartite genes

E14.5Bip promoters were more accessible than E14.5Biv promoters, and displayed similar accessibility as E14.5AcP genes (Fig. 4a, ATAC-seq and H3K27ac). Moreover, non-Bip genes with low, Bip-matching, levels of productive mRNA transcription (Fig. 4a, E14.5mRNALow;

Methods) displayed much lower promoter accessibility and H3K27ac levels than E14.5Bip promoters (Fig. 4a). Unlike E14.5Bip and E14.5Biv, E14.5mRNALow and E14.5AcP genes were not marked by H3K27me3 on gene body (Fig. 4a). Moreover, E14.5Bip promoters carried higher levels of the histone variant H3.3, involved in histone turn-over at transcriptionally active genes in postmitotic neurons[16], than E14.5Biv promoters (Fig. 4a). Furthermore, promoter Cdk9 levels of E14.5Bip genes were higher than E14.5Biv genes, and comparable with E14.5AcP genes (Fig. 4a). Cdk9 is a core component of pTEFb that catalyzes phosphorylation of RNAPII-S2 to regulate the transition from paused RNAPII (S5P form) to elongation (S2P form)[17] and its recruitment to enhancers and promoters requires H3K27 acetylation[18,19].

Furthermore, we then correlated the dynamics of elongation marks (RNAPII-S7P, RNAPII-S2P, H3K36me3) and other chromatin features (ATAC-seq, H3K4me2, H3K27ac, H3K27me3) with the transcriptional state of E14.5Bip genes through E18.5 and P4 development. Genes that become activated (E14.5Bip->P4Exp) displayed specifically increased levels of RNAPII-S7P, -S2P and H3K36me3 marks at P4 compared to E14.5Bip->P4Bip and E14.5Bip->P4Biv genes (Extended Data Fig. 6a, e). These results further support that the bipartite chromatin signature is consistently inversely correlated with the productivity of mRNA elongation of bipartite genes.

IEG bipartite chromatin is necessary to prevent precocious activity-dependent neuronal maturation during development

We asked whether preventing the establishment of the Pc bipartite signature on inducible IEGs *in vivo* during development may have a profound impact on the cell maturation program. Activity-regulated AP-1 family TFs (e.g. Fos, Jun) mediate the maturation process of early postnatal neurons through the *de novo* activation of AP-1-specific enhancers in a neuronal subtype-specific manner[20]. We hypothesized that the precocious activation of bipartite IEG-TFs, including Fos, in immature neurons by the removal of the gene body H3K27me3 mark may lead to precocious opening and activation of the early postnatal Fos-specific enhancer maturation program. Among the enhancers that normally become open only in postnatal barrelette neurons (3967 enhancers), we identified 85 neuronal activity-regulated Fos-binding enhancers[14] (see Methods). Interestingly, these 85 Fos-binding enhancers gained precocious accessibility in E14.5 *Ezh2cKO*$^{HB\text{-}RFP}$ homozygous mutant neurons (Fig. 5d, Extended Data Fig. 8b). In a complementary approach, we

next assessed that these 85 Fos-binding enhancers also gained accessibility in response to neuronal stimulation of E12.5 short-term cultured hindbrain trigeminal sensory neurons (Extended Data Fig. 8a; Methods), thus likely as a direct result of Fos induction. Together with the untimely expression of bipartite IEGs in *Ezh2cKO* embryonic sensory neurons at early stages (Fig. 5b), these results strongly suggests that functional inactivation of *Ezh2* could have an impact on prenatal neuronal development and maturation *in vivo*, at least in part, through ectopic up-regulation of activity-dependent bipartite IEGs and precocious activation of the early postnatal Fos-driven enhancer program.

Additional analysis of bipartite gene transcriptional regulation in PRC2 KO ESCs

To overcome the unfeasibility of obtaining large amounts of cells from *Ezh2cKO* embryos, we utilized *EedKO* mouse ESCs in which the H3K27me3 mark is removed genome-wide[21]. We carried out RNAPII-S2P ChIP-seq and mRNA-seq in wild-type and *EedKO* ESCs. RNAPII-S2P ChIP-seq signals have a narrower dynamic range (bottom 30% and top 30% expressed genes, Fig. 4a, b) compared to other RNAPII phosphorylated forms, likely because elongating RNAPII-S2P is a small fraction of total RNAPII. To improve the robustness of our analysis and to extend the general value of its conclusions, we considered all genes (n=3457) carrying H3K27me3 on their gene bodies rather than focusing only on 100-200 bipartite genes. For all these Pc targets, up-regulation of mRNA levels correlated with modest but significant increase of RNAPII-S2P signals in the TES region, in *EedKO* compared with wild-type ESCs (Extended Data Fig. 7f, g).

Next, we addressed whether it is H3K27 methylation and/or recruitment of Pc to the gene body that is essential for inhibition of bipartite mRNA transcription. We mined published datasets and analyzed the transcriptional changes of bipartite genes in full *Ezh1KO;Ezh2KO* and Ezh2 catalytically inactive *Ezh1KO;Ezh2*^{Y726D} mutant ESCs[22]. In *Ezh1KO;Ezh2KO* double mutant ESCs, PRC2-targeted genes lack both PRC2 binding and the H3K27me3 mark. In contrast, in *Ezh1KO;Ezh2*^{Y726D} ESCs, while the H3K27me3 mark was depleted PRC2 recruitment was rescued[22]. We found that bipartite genes are up-regulated in both full *Ezh1KO;Ezh2KO* and Ezh2 catalytically inactive *Ezh1KO;Ezh2*^{Y726D} ESCs (Extended Data Fig. 7h), indicating that the H3K27me3 mark itself on the gene body is fundamental for bipartite gene transcriptional regulation, rather than recruitment of PRC2 proteins.

Taken together, these results (and those presented in the main manuscript) strongly associate the Ezh2-dependent H3K27me3 marking of the gene bodies of bipartite genes to the inhibition of productive mRNA elongation. Furthermore, these data suggest a general involvement of the H3K27me3 mark on gene bodies in the regulation of productive mRNA elongation, beyond just bipartite genes.

Polycomb marking of bipartite genes bodies hampers productive elongation through inhibition of stimulus-dependent NELF release and chromatin compaction

The negative elongation factor (NELF) negatively regulates transcriptional elongation by pausing RNAPII at TSSs[23]. Stimulus-dependent NELF removal from IEG promoters causes release of paused RNAPII into elongation[24]. We hypothesized that H3K27me3 on gene body may inhibit transcriptional elongation in bipartite genes by interfering with stimulus-dependent NELF release. Indeed, the levels of NELF-b, a core component of the NELF complex, in bipartite gene promoters were decreased in *EedKO* compared to wild-type ESCs (Fig. 6a, left). Importantly, this was accompanied by the release of paused RNAPII-S5P from promoter regions (Fig. 6a, right), phenocopying the consequences of NELF knock-down experiments[25,26]. Together with the finding that the Pc marking of gene bodies of bipartite IEGs limits the extent of rapid stimulus-induced transcription (Fig. 5f,g), these results strongly indicate that H3K27me3 in bipartite gene bodies interferes with RNAPII release and elongation in part by inhibiting stimulus-dependent NELF removal.

There is evidence that PRC1 interferes with transcriptional elongation through chromatin compaction[27,28]. One unique feature of the bipartite signature is a high-level deposition of Ring1b, a core component of PRC1, in bipartite gene bodies (Fig. 4a). To assess the involvement of H3K27me3 in Ring1b bipartite gene body deposition and in gene body compaction (i.e. accessibility) we analyzed ChIP-seq of Ring1b and ATAC-seq in wild-type and *Ezh1KO;Ezh2KO* mouse ESCs from published datasets[22]. We found that *Ezh1/Ezh2* removal caused a reduction of gene body Ring1b levels in bipartite genes (Fig. 6b), indicating that the gene body Ring1b deposition on bipartite genes is H3K27me3-dependent. This correlated with significant increase of bipartite gene body, though not promoter, accessibility in *Ezh1KO;Ezh2KO* mouse ESCs (Fig. 6c).

We next asked if the de-compaction (increased accessibility) of bipartite genes in PRC2 KO was primarily caused by the removal of H3K27me3 per se or whether it was merely a consequence of increased transcription. We carried out experiments to quantify chromatin compaction of bipartite IEGs (i.e. *Fos*, *Egr1*) using wild-type and *EedKO* ESCs in the serum-starved condition (Fig. 6d, e). While these IEGs showed a modest increase of expression in *EedKO* ESCs, as compared to wild-type, in the serum-containing medium (Fig. 6d, mRNA), in the serum-starved condition they were basically not expressed (Fig. 6e, mRNA; also see Fig. 5f), likely due to lack of inducing stimulus. We found that even in the serum-starved condition bipartite IEG gene bodies showed increased accessibilities in *EedKO* ESCs (Fig. 6e, ATAC), indicating that the de-compaction of bipartite gene bodies was not only merely correlative with increased transcription, but was also at least partially caused by PRC2 deletion and the removal of H3K27me3.

Stimulus-dependent H3K27me3 removal from IEG gene bodies requires active de-methylation

GSK-J4, an inhibitor of H3K27me3 demethylases (i.e. UTX (Kdm6a), Jmjd3 (Kdm6b)) prevented neuronal activity-dependent gene body H3K27me3 removal (Fig. 7d), indicating that H3K27me3 is removed through active demethylation. ChIP-seq of H3K27me3 in E18.5 wild-type and *Jmjd3KO* (Supplementary Table 1, Methods) hindbrain confirmed that inactivation of *Jmjd3* inhibited, at least partially, removal of the gene body H3K27me3 mark from the E14.5 bipartite genes that become active at peri/postnatal (P4) stages (Fig. 7e). These results strongly indicate that the stimulus-dependent removal of H3K27me3 from IEG gene bodies requires active de-methylation.

Effect of A-485 treatment on transcriptional induction of bipartite IEGs

We assessed the effect of A-485 treatment on neuronal activity-dependent transcriptional induction of bipartite IEGs. A-485 treatment prevents the rapid induction of bipartite IEGs after short-time (i.e. 8 minutes) exposure to KCl (Fig. 7h). Taken together with the effects of the H3K27me3 demethylase inhibitor (i.e. Gsk-J4) treatment on the rapid induction of bipartite IEGs (Fig. 7f), this result strongly indicates that fast bipartite IEG transcriptional induction requires *de novo* H3K27acetylation and rapid removal of the gene body H3K27me3 mark through active de-methylation (Fig. 7i, scheme).

On the other hand, after prolonged exposure (i.e. 60 minutes) to the KCl stimulus even A-485 treated neurons showed transcriptional up-regulation of bipartite IEGs. However, as is the case with the H3K27me3 demethylase inhibitor (Fig. 7f), mRNA levels remained significantly lower as compared to control neurons (Fig. 7g). This indicates that, even in the event of lack of H3K27ac increase at the bipartite IEG promoters, the existing H3K27ac levels are sufficient to allow the mRNA of bipartite IEGs to accumulate over time upon prolonged stimulation, albeit their transcripts do not reach optimal levels under such a condition (Fig. 7i, scheme).

KCl-dependent gene body H3K27me3 removal is driven by de novo promoter acetylation per se irrespective of transcriptional elongation

We asked whether the KCl-dependent gene body H3K27me3 removal is the consequence of transcriptional elongation or rather it is driven by promoter acetylation per se. We treated E12.5 short-term cultured neurons with KCl in the presence of flavopiridol, a Cdk9 inhibitor. Flavopiridol treatment caused a complete block of the KCl-dependent transcription of IEGs, while *de novo* promoter H3K27ac was not prevented (Fig. 7j). Interestingly, we found that flavopiridol did not prevent the KCl-dependent removal of H3K27me3 from bipartite IEG gene bodies (Fig. 7j), indicating that the gene body H3K27me3 mark is removed by KCl-induced neuronal stimulation regardless of mRNA transcriptional elongation, provided that *de novo* promoter H3K27 acetylation occurs.

Supplementary Discussion

We first investigated how the bipartite signature is established, maintained, and resolved during development. Bipartite genes are established in a cell type- and developmental stage-specific manner and constitute a small but consistent fraction (5-15%) of the bivalent genes (Figs. 2a, d and 3a-d), suggesting that the transition of a subset of bivalent genes into a bipartite state may depend on the distinct environmental conditions to which developing cells in different tissues are exposed. Indeed, in addition to typical stimulus response IEGs, bipartite genes encode for cell-type specific transcriptional regulators, receptors, and molecules responding to distinct signaling pathways (Fig. 2c).

We show that, unlike the more stable bivalent chromatin, the bipartite state allows for dynamic and reversible (i.e. from bivalent to bipartite to bivalent, or to active, state) chromatin changes through developmental stages and that this correlates with transcriptional output changes (Fig. 3, Extended Data Fig. 6a). The initial transition from bivalent to bipartite chromatin in different cell types and/or developmental stages might be regulated by specific sets of transcription factors. For instance, we show that in barrelette neurons at E14.5, the E14.5Bip gene promoters are enriched for NF-kB-related and forkhead FOX-related factor binding motifs (Extended Data Fig. 3g), suggesting that they might be involved in the transition leading to partial resolution of bivalency into a bipartite state. Once established, the bipartite signature is maintained through a reciprocal competitive balance between H3K27ac at promoters and H3K27me3 in gene bodies (Figs. 3d, 5a and 7a-k). In this respect, it is noteworthy that HDAC levels shuttling between the nucleus and cytoplasm can be signal-regulated[29].

As for the transition from the bipartite to active state, we found that pCREB binding levels increased in promoter (and enhancer, e.g. at *Fos* locus, Fig. 3e) regions of stimulus response genes that were bipartite at E14.5 and became active at E18.5/P4 (Fig. 3e, 7a), including neuronal activity-induced IEGs (Fig. 3e, Extended Data Fig. 6b,d). Increase of stimulus-dependent phosphorylation of CREB and subsequent increase of acetylation of H3K27 causes active H3K27me3 demethylation from bipartite gene bodies and elongation barrier release, correlating with bipartite chromatin resolution into an active state and productive transcription (Fig. 7a-k, summary diagram Fig. 8). Conversely, decrease of pCREB levels on E14.5Bip genes correlated with reversion into bivalency at P4 (Fig. 7a). Thus, while NF-kB and/or FOX factors might initially

increase the accessibility at E14.5Bip promoters contributing to partial resolution of bivalency and transition into the bipartite state, stimulus-dependent CREB phosphorylation binding levels might serve as an environmental sensor and a rheostat to bi-directionally regulate the balance between H3K27ac and H3K27me3 at bipartite target gene loci.

The bipartite state can be resolved into further repression or activation, a feature also shared with the bivalent state. However, unlike the bivalent state, we demonstrate that the bipartite chromatin still enables very rapid transcriptional inducibility of stimulus response genes, while integrating both levels and duration of the signal (Fig. 5f,g). How fast, when, or whether at all, a stimulus response gene might be transcriptionally induced by any given environmental signal that cells may experience during development has obviously an important impact on cell fate decisions and downstream transcriptional programs of maturation. We speculate that the bipartite chromatin provides a unique epigenetic mechanism regulating transcriptional sensitivity of target genes to different signals, ultimately resulting in context-dependent interpretation of signal relevance by the developing cell. In addition to molecular mechanisms regulating the competence of a cell to receiving the signal[30], we reveal a mechanism acting directly at stimulus response genes and providing competence to respond to the signal through their active promoter state, while maintaining epigenetic control on the timing and level of transcriptional response through the repressive Pc marking of the gene body (summary diagram, Fig. 5g), thus providing a way to evaluate signal relevance during development. During development, this chromatin structure at immediate early stimulus response genes might be most effective in preventing inappropriate induction by acute exposure to weak or non-physiologically relevant signals. In fact, based on our results (Fig. 7b-i), it is likely that short exposure to an inducing signal could achieve fast bipartite IEG transcriptional induction only if signal levels are sufficiently high to induce fast increase of promoter H3K27 acetylation and fast gene body H3K27me3 removal.

As for the molecular mechanism underlying the transcriptional regulation of bipartite genes, analysis of the distribution of RNAPII phosphorylated forms on bipartite genes revealed that at the stages when H3K27me3 levels on gene bodies are relatively high and bipartite genes are not or barely productively transcribed, RNAPII-S5P and RNAPII-S7P appear to be pausing at the promoter-proximal first exon regions, while both RNAPII-S7P and RNAPII-S2P signals are negligible in the gene body regions (Fig. 4a,b, Extended Data Fig. 6d). Indeed, some IEGs, including *Fos* and *Egr1*, are known to be regulated by RNAPII pausing in early elongation, and

by controlled, stimulus-dependent, release of paused RNAPII into productive RNA synthesis[31]. In particular, at the human *Fos* locus, RNAPII pauses within the first 300 nucleotides of the first exon[31]. This is compatible with the localization of RNAPII-S5P and -S7P peaks at the mouse *Fos* locus in developing E14.5 hindbrain tissue and ESCs (Extended Data Figs. 6d and 7g). On the other hand, the finding of RNAPII pausing on bipartite genes was intriguing; in fact, genes in a bipartite state are not or very lowly productively expressed, yet RNAPII pausing has been mainly observed on expressed genes[32]. Interestingly, this reminds of a particular class of 'paused and inactive' genes representing only < 2% of all genes (class III in Min et al., 2011[32]). This number is roughly compatible with the low number of bipartite genes we observe during development. It is therefore tempting to speculate that, during development, this class might be represented by the bipartite genes.

At the bipartite stage, RNAPII does not efficiently transit into productive elongation. At later stages, correlating with significant reduction or loss of H3K27me3 on gene bodies, we observed increasing accumulation of elongation marks (RNAPII-S7P, RNAPII-S2P, and H3K36me3) at the bipartite loci resolving into transcriptional activation. In developing neurons, this is driven by stimulus-dependent accumulation of pCREB and H3K27ac signals at promoters and enhancers (see above).

Functional analysis in developing hindbrain neurons and ESCs strongly supported a role of PRC2-dependent H3K27me3 marking of gene bodies in inhibiting RNAPII-dependent transcript elongation (Figs. 5 and 6, Extended Data Fig. 7, summary diagram Fig. 8). This is directly supported by the increase of elongation mark levels in PRC2 knockout mutants both in hindbrain neurons and ESCs (Extended Data Fig. 7e-g). Pc-dependent inhibition of productive mRNA elongation in bipartite IEGs may be achieved by multiple mechanisms including inhibition of stimulus-induced release of the NELF complex and chromatin compaction limiting RNAPII elongation. Indeed, we found that the H3K27me3 in bipartite gene bodies of bipartite IEGs limits the extent of rapid stimulus-induced transcription (Fig. 5f, g), as well as the release of both the NELF complex and of transcriptionally initiating RNAPII (Fig. 6a) at promoters. The Cdk9 binding profile (Fig. 4a), the increased gene body accessibility correlating with developmental removal of H3K27me3 (Extended Data Fig. 6a), the finding that the H3K27me3 mark in gene bodies of bipartite genes serves as a platform to recruit high levels of PRC1 (i.e. Ring1b, Figs. 4a and 6b), that elongation is not required for Eed deletion to increase chromatin accessibility and

that H3K27me3 (or Eed) is required for full compaction (Fig. 6c-e), further suggested that the poor mRNA elongation of bipartite genes may be additionally due to impairment of RNAPII to physically go through a Pc-compacted gene body chromatin.

Lastly, in prenatal postmitotic barrelette neurons, the bipartite state might critically prepare IEGs to rapidly respond to sensory (e.g. whisker) stimuli at the beginning of the critical period by activity-dependent increase of productive mRNA elongation. Active promoters and enhancers of bipartite genes, and high levels of pre-loaded RNAPII at bipartite gene promoters, might enable synchronous patterns of stimulus-dependent IEG transcription in response to whisker stimulus-specific correlated activity, which is critical to precisely refine the whisker-related barrelette map[8]. Moreover, we speculate that Pc-dependent epigenetic regulation at gene bodies of stimulus-inducible genes at prenatal stages might 'pre-label' gene bodies for further epigenetic marking in postnatal mature neurons replacing the developmental Pc marking pattern, such as e.g. gene body DNA methylation and recruitment of Mecp2[33], that is known to also cause chromatin compaction of targeted genomic regions[34].

Supplementary Methods

Animals

All animal experimental procedures were performed in accordance with Guide for Care and Use of Laboratory Animals, and were approved by the Veterinary Department of the Canton of Basel-Stadt.

Generation of the r2::EGFP mouse line

To generate the *r2::EGFP* (*r2*$^{EGFP/+}$) mouse line, an *EGFP* cassette (Clontech) was used to generate a pKS-β-globin-EGFP plasmid. The BamH1 2.5 kb rhombomere 2-specific enhancer of *Hoxa2*[35] was then cloned in reverse orientation 5′ of the β-globin promoter, thus generating a final construct consisting of the r2-specific enhancer, a β-globin minimal promoter, and *EGFP* encoding sequence. The construct was linearized, purified, and microinjected into the pronuclei of mouse zygotes. Founders were identified by PCR.

Mouse embryonic hindbrain neuron cultures

E12.5 CD1 wild-type or *Drg11*$^{tdTomato/+}$ mouse embryo hindbrains were dissected, and treated with 0.05% Trypsin/EDTA (Thermo Fisher Scientific, 25300054) for 3 minutes at 37°C, rinsed by ice-cold DMEM 1X, and dissociated by pipetting. Cells were seeded on dishes (Day0). Dishes were pre-coated over-night by collagen I (Thermo Fisher Scientific, A1048301) in PBS 1X. Neurons were maintained in Neurobasal Medium (Thermo Fisher Scientific, 21103049) containing 2% B27 Supplement (Thermo Fisher Scientific, A3582801), 2% GlutaMAX Supplement (Thermo Fisher Scientific, 35050061) and penicillin-streptomycin. For a long culture (upto 1 week), medium was changed every two day.

Mouse embryonic stem cells (ESCs) cultures

Mouse embryonic stem cells (ESCs) were cultured in the culture medium containing DMEM (Thermo Fisher Scientific, 41965), 55μM 2-Mercaptoethanol (Thermo Fisher Scientific, 21985023), 2% GlutaMAX Supplement (Thermo Fisher Scientific, 35050061), 1X MEM Non-Essential Amino Acids solution (Thermo Fisher Scientific, 11140050), 1000 unit/ml ESGRO

Recombinant Mouse LIF Protein (Merck, ESG1106), penicillin-streptomycin and 15% FCS. Dishes were pre-coated by 0.1% gelatin (Sigma, G2500).

Sample preparation, chromatin immunoprecipitation (ChIP) and sequencing (ChIP-seq)

ChIPmentation of the FACS-sorted cells

For ChIP-seq experiments using FACS-sorted cells, dissociated tissue was cross-linked with 1% formaldehyde in DMEM 1X/ FCS 10% for 10 minutes at room temperature (RT) and quenched with 125mM glycine for 5 minutes at RT. Cells were pelleted by centrifugation (1500 rcf, 5 minutes, 4°C) and rinsed twice with PBS 1X/ FCS 4%. Cells were filtered and collected by FACS. For each experiment, two to three independent biological replicates were used. To achieve the sequencing of chromatin immunoprecipitated from small amount of cells, preparation of ChIP-seq library was done by ChIPmentation protocol [36]. 50,000 cells (H3K4me2, H3.3) and 100,000 – 200,000 cells (H3K27ac, H3K27me3) were used. Cells were lysed in 20 – 40µl of Sonication Buffer (10mM Tris HCl pH8, 5mM EDTA, 0.5% SDS, 0.1X PBS, 1X Protease Inhibitor Cocktail (PIC – cOmplete – EDTA free, Roche, 04693132001)) for 15 min on ice, and sonicated using the Covaris machine to obtain DNA fragment the size of which distributes between 150bp and 500bp. The supernatant was transferred to a new tube, diluted five times with Equilibration Buffer (10mM Tris HCl pH8, 1mM EDTA, 140mM NaCl, 1% Triton X-100, 0.1% Sodium deoxycholate, 1X Protease Inhibitor Cocktail). Chromatin solutions were incubated over-night at 4°C with 1µg of anti-H3K4me2 (Millipore, 07-030, PRID: AB_10099880), 1µg of anti-H3K27ac (abcam, ab4729, PRID: AB_2118291), 1µg of anti-H3K27me3 (Millipore, 07-449, PRID: AB_310624) or 1µg anti-H3.3 (Millipore, 09-838, PRID: AB_10845793) antibodies. The next day, 20µl of protein G coupled to magnetic beads (Dynabeads Protein G, Thermo Fisher, 10004D) were added and the incubation was continued for 2 hours at 4°C. The beads were then washed five times with RIPA Buffer (10mM Tris HCl pH8, 1mM EDTA, 140mM NaCl, 1% Triton X-100, 0.1% SDS, 0.1% Sodium deoxycholate, 1X Protease Inhibitor Cocktail), twice with High-Salt RIPA Buffer (10mM Tris HCl pH8, 1mM EDTA, 500mM NaCl, 1% Triton X-100, 0.1% SDS, 0.1% Sodium deoxycholate, 1X Protease Inhibitor Cocktail), twice with LiCl Buffer (10mM Tris HCl pH8, 1mM EDTA, 250mM LiCl, 0.5% NP40, 0.5% Sodium deoxycholate, 1X Protease Inhibitor Cocktail), and twice with 10mM Tris HCl pH8. Beads were resuspended in 30µl Tagmentation Buffer (10mM Tris HCl pH8, 5mM $MgCl_2$) containing 1µl Tagment DNA Enzyme from the Nextera

DNA Sample Prep Kit (Illumina, FC-121-1030) and incubated at 37°C for 10min. The beads were washed twice with RIPA Buffer and twice with TE Buffer (10mM Tris HCl pH8, 1mM EDTA). DNA was eluted from the beads with 60µl Elution Buffer (10mM Tris HCl pH8, 5mM EDTA, 300mM NaCl, 0.5% SDS, proteinase K) at 65°C for 5hours. DNA was purified with SPRI AMPure XP beads (Beckman, sample to beads ratio 1:2) and eluted in 25µl 10mM Tris HCl pH8. 2µl of each library was amplified in 10µl qPCR reaction (1X Sybr Green (Thermo Fisher), 0.8µM primers, 1X KAPA HiFi Hot Start Ready Mix (Kapa Biosystems): StepOnePlus Real-Time PCR Systems (Thermo Fisher), 72°C for 5min; 98°C for 1min; 25 cycles of 98°C for 15sec, 63°C for 30sec, 72°C for 1min) to estimate the optimum number of enrichment cycles. Final enrichment of the libraries was performed in 50µl reaction (1X KAPA HiFi Hot Start Ready Mix and 0.8µM primers). Enriched libraries were purified with size selection using SPRI AMPure XP beads (sample to beads ratio 1:0.6) to remove long fragments, recovering the remaining DNA (sample to beads ratio 1:2). Sequencing was performed on an Illumina HiSeq 2500 machine (50bp read length, single-end).

ChIPmentation of bulk tissue

For ChIP-seq experiments using wild-type brainstem tissue and cultured embryonic hindbrain neurons dissociated tissue was cross-linked with 1% formaldehyde in PBS 1X for 10 minutes at room temperature (RT) and quenched with 125mM glycine for 5 minutes at RT. Cells were pelleted by centrifugation (1500 rcf, 5 minutes, 4°C) and rinsed twice with PBS 1X/ FCS 4%, and cells were filtered. Normally we prepare at least two biological replicate, but for some experiments of bulk ChIP-seq, independent biological replicates were not prepared, but analysis were supported by the use of internal controls and the sample was normalized and compared with samples from related condition (see below). Preparation of ChIP-seq library was done by ChIPmentation protocol, except for ChIP-seq of the H3K27ac marks of control and TSA-treated cultured E12.5 hindbrain neurons that were prepared according to manufacturer's protocol of NEBNext Ultra DNA Library Prep Kit for Illumina (NEB, E7370) 1,000,000 cells (H3K36me3), 5,000,000 cells (phospho-CREB (pCREB), non-phosphorylated RNAPII 8WG16, Ring1b) or 30,000,000 cells (Ser5P RNAPII, Ser7P RNAPII, Ser2P RNAPII, Cdk9) were used. Cells were lysed in 200 - 800 µl of Sonication Buffer (10mM Tris HCl pH8, 5mM EDTA, 0.15% SDS, 0.1X PBS, 1X Protease Inhibitor Cocktail) for 15 min on ice, and sonicated using the Covaris machine or the Bioruptor Pico machine to obtain DNA fragment the size of which distributes between 150bp and 500bp.

After centrifugation (1 min, 10,000rpm, 4°C), the supernatant was transferred to new tubes, diluted five times with Equilibration Buffer. Chromatin solutions were incubated over-night at 4°C with 1µg of anti-H3K36me3 (abcam, ab9050, PRID: AB_306966), 10µg of anti-pCREB (Millipore, 17-10131, PRID: AB_10807817), 10µg of anti-Ring1b (Cell Signaling, 5694, PRID: AB_10705604), 10µg of anti-non-phosphorylated RNAPII 8WG16 (Covance, MMS-126R, PRID: AB_10013665), 30µg of anti-Ser5P RNAPII 4H8 (Covance, MMS-128P, PRID: AB_10013820), 30µg of anti-Ser7P RNAPII 4E12 (Millipore, 04-1570, PRID: AB_10618152), 30µg of anti-Ser2P RNAPII 3E10 (Active Motif, 61083, PRID: AB_2687450) and 30µg of anti-Cdk9 (abcam, ab239364) antibodies. The next day, 40 - 200 µl of protein G coupled to magnetic beads were added and the incubation was continued for 2 hours at 4°C (as for anti-Ser7P RNAPII 4E12 and Ser2P RNAPII 3E10 rat-derived IgG_1, 200µl beads were pre-incubated with 60µl rabbit-derived anti-rat IgG antibody (abcam, ab6703, PRID: AB_956015) over-night to bridge primary antibodies and protein G). The beads were then washed twice with RIPA Buffer, once with High-Salt RIPA Buffer, once with LiCl Buffer, and twice with 10mM Tris HCl pH8. Beads were resuspended in 30-90µl Tagmentation Buffer containing 1-3µl Tagment DNA Enzyme and incubated at 37°C for 10min. The beads were washed twice with RIPA Buffer and twice with TE Buffer. DNA was eluted from the beads with 60µl Elution Buffer at 65°C for 5hours. DNA was purified with SPRI AMPure XP beads (sample to beads ratio 1:2) and eluted in 25µl 10mM Tris HCl pH8. 2µl of each library was amplified in 10µl qPCR reaction to estimate the optimum number of enrichment cycles. Final enrichment of the libraries was performed in 50µl reaction. Enriched libraries were purified with size selection using SPRI AMPure XP beads (sample to beads ratio 1:0.6) to remove long fragments, recovering the remaining DNA (sample to beads ratio 1:2). Sequencing was performed on an Illumina HiSeq 2500 machine (50bp read length, single-end).

ChIPmentation of tissues pre-fixed prior to dissociation

To avoid any effects of dissociation on chromatin state, we performed ChIP-seq against H3K27ac and H3K27me3 using E14.5 PrV tissue that was pre-fixed prior to dissociation. For this, micro-dissected PrV region was directly cross-linked with 1% formaldehyde in DMEM 1X/ FCS 10% for 12 minutes at room temperature (RT) and quenched with 125mM glycine for 5 minutes at RT. The tissue was rinsed twice with DMEM 1X/ FCS 4% and once with PBS, then treated with papain digestion mix for 15 minutes at 37°C and immediately put on ice. Tissue was rinsed by ice-cold DMEM 1X, and dissociated by pipetting and filtered. 500,000 cells were used per ChIP, and

reparation of library was done by ChIPmentation protocol as described above. We prepared only one biological replicate for each mark, but they were enough to confirm existence of the bipartite signature in IEGs.

Sequential (Double) ChIP-seq (H3K27me3/H3K27ac) of large chromatin fragments (Extended Data Fig. 4a)

For single ChIP-seq against H3K27ac or H3K27me3, or for sequential H3K27me3/H3K27ac ChIP-seq experiments with large (2-3kb) chromatin fragments, E14.5 wild-type brainstem tissue was dissociated and cross-linked with 1% formaldehyde in PBS 1X for 10 minutes at room temperature (RT) and quenched with 125mM glycine for 5 minutes at RT. Cells were pelleted by centrifugation (1500 rcf, 5 minutes, 4°C) and rinsed twice with PBS 1X/ FCS 4%, and cells were filtered. Six million cells were used. Cells were lysed in 200 µl of Sonication Buffer (10mM Tris HCl pH8, 5mM EDTA, 0.5% SDS, 0.1X PBS, 1X Protease Inhibitor Cocktail (PIC – cOmplete – EDTA free, Roche)) for 15 min on ice, and sonicated using the Bioruptor Pico machine to obtain DNA fragment the size of which distributes around 2kb. After centrifugation (1 min, 10,000rpm, 4°C), the supernatant was transferred to new tubes, diluted ten times with Equilibration Buffer. Samples were pre-cleaned by protein G coupled to magnetic beads at 4°C for one hour. As for single ChIP-seq, 10% of chromatin was incubated over-night at 4°C with 1µg of anti-H3K27ac or anti-H3K27me3 antibodies. The next day, 20µl of protein G coupled to magnetic beads were added and the incubation was continued for 2 hours at 4°C. The beads were then washed twice times with RIPA Buffer, once with High-Salt RIPA Buffer, once with LiCl Buffer, and once with TE Buffer. DNA was eluted from the beads with 100µl Elution Buffer at 65°C for over-night. DNA was purified with MinElute PCR Purification Kit (QIAGEN, 28004). As for sequential ChIP-seq, remaining chromatin was incubated over-night at 4°C with 5µg of anti-H3K27me3 antibody. The next day, 100µl of protein G coupled to magnetic beads were added and the incubation was continued for 2 hours at 4°C. The beads were then washed twice with RIPA Buffer, once with High-Salt RIPA Buffer, once with LiCl Buffer, and once with TE Buffer. To release chromatin from beads, DTT, high salt and detergent were used. Firstly beads were incubated with 50µl DTT 100mM at room temperature for 10 minutes, then 50µl 2X Chromatin Release Buffer (500mM NaCl, 2% SDS, 2% sodium deoxychorate, 2X Protease Inhibitor Cocktail) were added and mixed thoroughly and incubate at 37°C for 50 minutes. Magnetic beads were removed and samples were diluted four times by Equilibration Buffer, and concentrated using a 50Kda cutoff Amicon Ultra-

0.5 mL (Merck, FC505024). The collected samples were then further diluted ten times by Equilibration Buffer, and pre-cleaned by protein G coupled to magnetic beads at 4°C for one hour twice. Then samples were incubated over-night at 4°C with 1µg of anti-H3K27ac antibody. The next day, 20µl of protein G coupled to magnetic beads were added and the incubation was continued for 2 hours at 4°C. The beads were then washed twice with RIPA Buffer, once with High-Salt RIPA Buffer, once with LiCl Buffer, and once with TE Buffer. DNA was eluted from the beads with 100µl Elution Buffer at 65°C for over-night. DNA was purified with MinElute PCR Purification Kit. For both the single and sequential ChIP-seq, purified large fragments (2kb) of DNA were fragmented by 1µl Tagment DNA Enzyme from the Nextera DNA Sample Prep Kit (Illumina) at 55°C for 5 minutes. After tagmentation, DNA was purified with MinElute PCR Purification Kit by 25µl 10mM Tris HCl pH8. 2µl of each library was amplified in 10µl qPCR reaction to estimate the optimum number of enrichment cycles. Final enrichment of the libraries was performed in 50µl reaction. Enriched libraries were purified with size selection using SPRI AMPure XP beads (sample to beads ratio 1:0.6) to remove long fragments, recovering the remaining DNA (sample to beads ratio 1:2). Sequencing was performed on an Illumina HiSeq 2500 machine (50bp read length, single-end). Sequential ChIP-seq were prepared with two independent biological replicates. Long fragment single-mark ChIP-seq were prepared without replicates, but a bipartite chromatin pattern was clearly visible in these samples.

ChIPmentation of mouse ESCs

Mouse ESCs were cross-linked with 1% formaldehyde in DMEM 1X for 10 minutes at room temperature (RT) and quenched with 125mM glycine for 5 minutes at RT. Cells were rinsed twice with PBS 1X/ FCS 4% and collected by scraping. Normally we prepare at least two biological replicate, but for some experiments of bulk ChIP-seq, independent biological replicates were not prepared, but analysis were supported by the use of internal controls and the sample was normalized and compared with samples from related condition (see below). Preparation of ChIP-seq library was done by ChIPmentation protocol. 1,000,000 cells (H3K4me2, H3K27ac, H3K27me3), or 30,000,000 cells (Ser5P RNAPII-S5P, Ser2P RNAPII, NELF-b) were used. Cells were lysed in 200 - 800 µl of Sonication Buffer (10mM Tris HCl pH8, 5mM EDTA, 0.15% SDS, 0.1X PBS, 1X Protease Inhibitor Cocktail) for 15 min on ice, and sonicated using the Covaris machine or the Bioruptor Pico machine to obtain DNA fragment the size of which distributes between 150bp and 500bp. After centrifugation (1 min, 10,000rpm, 4°C), the supernatant was

transferred to new tubes, diluted five times with Equilibration Buffer. Chromatin solutions were incubated over-night at 4°C with 5µg of anti-H3K4me2 (Millipore, 07-030, PRID: AB_10099880), 5µg of anti-H3K27ac (abcam, ab4729, PRID: AB_2118291), 6µg of anti-H3K27me3 (Cell Signaling, 9733, PRID: AB_2616029), 30µg of anti-Ser5P RNAPII 4H8 (Covance, MMS-128P, PRID: AB_10013820), 30µg of anti-Ser2P RNAPII 3E10 (Active Motif, 61083, PRID: AB_2687450) and 30 µg of anti-NELF-b (abcam, ab237027) antibodies. The next day, 40 - 200 µl of protein G coupled to magnetic beads were added and the incubation was continued for 2 hours at 4°C (as for anti Ser2P RNAPII 3E10 rat-derived IgG_1, 200µl beads were pre-incubated with 60µl rabbit-derived anti-rat IgG antibody over-night to bridge primary antibodies and protein G). The beads were then washed twice with RIPA Buffer, and twice with 10mM Tris HCl pH8. Beads were resuspended in 30-90µl Tagmentation Buffer containing 1-3µl Tagment DNA Enzyme and incubated at 37°C for 10min. The beads were washed twice with RIPA Buffer and twice with TE Buffer. DNA was eluted from the beads with 60µl Elution Buffer at 65°C for 5hours. DNA was purified with SPRI AMPure XP beads (sample to beads ratio 1:2) and eluted in 25µl 10mM Tris HCl pH8. 2µl of each library was amplified in 10µl qPCR reaction to estimate the optimum number of enrichment cycles. Final enrichment of the libraries was performed in 50µl reaction. Enriched libraries were purified with size selection using SPRI AMPure XP beads (sample to beads ratio 1:0.6) to remove long fragments, recovering the remaining DNA (sample to beads ratio 1:2). Sequencing was performed on an Illumina HiSeq 2500 machine (50bp read length, single-end).

Sample preparation, RNA isolation and sequencing (RNA-seq)

For RNA-seq experiments, dissociated tissue was filtered and kept on ice until sorting. Sorted cells were collected into ice cold PBS 1X, and immediately pelleted by centrifugation (500 rcf, 5 minutes, 4°C). Total RNA was extracted by NORGEN Single Cell RNA Purification Kit (NORGEN, 51800) with genomic DNA digestion using RNase-Free DNase I Kit (NORGEN, 25710) according to manufacturer's protocol. For each experiment, three independent biological replicates were used.

Sequencing of poly A+ mRNA was done by Smart-seq2 protocol[37]. 1ng of total RNA was used as an input. Reverse transcription was conducted using 100U SuperScript II reverse transcriptase (Thermo Fisher, 18064014), 10U RNase inhibitor (Clontech, 2313A), 1X Superscript

II first-strand buffer, 5mM DTT (contained in SuperScript II reverse transcriptase), 1M Betaine (Sigma, B0300-1VL), 6mM MgCl2, 1µM template-switching oligos (TSOs) (exiqon), 1µM oligo-dT primer (Mycrosynth) and 1mM dNTP mix (Thermo Fisher, R0191) in total volume 10µl. Then PCR pre-amplification was done using 1X KAPA HiFi HotStart Ready Mix (KAPA Biosystems, KK2602), 0.1µM IS PCR primers (Mycrosynth) in total volume 25µl using 13 cycles of PCR. DNA was purified with SPRI AMPure XP beads (Beckman, sample to beads ratio 0.8:1) and eluted in 20µl 10mM Tris HCl pH8. Tagmentation reaction was done by Illumina Nextera XT DNA Library Prep Kit (Illumina, FC-131-1024) in total volume 5µl using 0.2ng DNA as an input, then amplification of adapter-ligated fragment was done using Illumina XT kits in a total volume 12.5µl with 12 cycles of PCR. Library was purified by SPRI AMPure XP beads (sample to beads ratio 0.6:1) and eluted in 12µl 10mM Tris HCl pH8. Sequencing was performed on an Illumina HiSeq 2500 machine (50bp read length, single-end).

Sequencing of total RNA was done by Ovation SoLo RNA-seq System (NuGEN, 0501-32), using 2.5 – 5ng of RNA as an input according to manufacturer's protocol. Sequencing was performed on an Illumina HiSeq 2500 machine (50bp read length, single-end).

Sample preparation and single-cell RNA sequencing (scRNA-seq)

To collect rhombomere 3 (r3)-derived progenitors from E10.5 *K20*$^{tdTomato/+}$ mouse, r2 – r4 regions were micro dissected. To collect E14.5 *Drg11*$^{vPrV\text{-}tdTomato/+}$ post-mitotic barrelette neurons from *Drg11*$^{tdTomato/+}$*;r2*$^{EGFP/+}$ mice, r2 – r3 derived regions were micro dissected. The boundary between r3 and r4 was identified by the position of the facial nerve. Dissected tissue was kept in PBS 1X containing 2µM actinomycin D (Sigma, A1410) for 10 minutes on ice, then treated with papain digestion mix (papain 10mg/ml/ cysteine 2.5mM/ HEPES pH7.4 10mM/ EDTA 0.5mM/ DMEM 0.9X/ 40µM actinomycin D) for 3 minutes at 37°C and immediately put on ice. Tissue was rinsed by ice-cold DMEM 1X containing 2µM actinomycin D, and dissociated by pipetting and filtered. r3-derived cells were collected by FACS (Extended Data Fig. 1d, Supplementary Figs. 1 and 2b).

Cells were sorted directly into 50µl of PBS-0.04%BSA. Cell concentration was determined using a TC20 automated cell counter (BioRad). As for E10.5 progenitors, 4,500 and 2,250 cells were respectively loaded into two different channels of a Chromium Single Cell A Chip (10X Genomics). As for E14.5 barrelette neurons, 8,000 cells were loaded into one channel of a Chromium Single Cell A Chip. Reverse-transcription, cDNA pre-amplification (13 cycles) and

library preparation were performed according to the manufacturer instructions (Chromium Single Cell 3′ Library & Gel Bead Kit v2, 10X Genomics). Libraries were sequenced on a Illumina NextSeq 500 platform (R1: 26bp, R2: 56bp, I1: 8bp). Demultiplexing and fastq files generation were performed using the CellRanger pipeline (10X Genomics).

Sample preparation and assay for transposase accessible chromatin (ATAC-seq)

Dissociated tissue was filtered and kept on ice until sorting. Two independent biological replicates were prepared. Sorted cells were collected into ice cold PBS 1X, and immediately pelleted by centrifugation (500 rcf, 5 minutes, 4°C). 50,000 – 70,000 cells were used for each experiment. Cells were washed once with 50µl PBS 1X and pelleted (500 rcf, 5 minutes, 4°C), and gently resuspended by pipetting in ice cold 50µl cold lysis buffer (10mM Tris HCl pH7.4, 10mM NaCl, 3mM $MgCl_2$, 0.1% IGEPAL CA-630) to extract nuclei and pelleted (500 rcf, 10 minutes, 4°C). Nuclei were washed once with ice cold 50µl Tagmentation Buffer (10mM Tris HCl pH8, 5mM $MgCl_2$) and pelleted (500 rcf, 10 minutes, 4°C). Then nuclei were tagmented in transposition reaction mix (2.5µl Tn5 Transposase (Illumina, FC-121-1030), 25µl 2X TD Buffer (Illumina, FC-121-1030), and 22.5µl nuclease free water) at 37°C for 30 minutes. DNA was purified with MinElute PCR Purification Kit (Qiagen, 28004) by 10µl 10mM Tris HCl pH8. Library amplification was started with 1X KAPA HiFi HotStart Ready Mix, 1.25µl primers and 0.6X Sybr Green (Thermo Fisher) in total volume 50µl: 72°C for 5min; 98°C for 1min; 5 cycles of 98°C for 15sec, 63°C for 30sec, 72°C for 1min. 5µl of 5 cycled DNA was taken and quantitative PCR was conducted to optimize PCR cycle (StepOnePlus Real-Time PCR Systems (Thermo Fisher)), and then remaining 45µl was further PCR amplified according to the necessity. DNA was purified with SPRI AMPure XP beads (Beckman, sample to beads ratio 1:2) and eluted in 20µl 10mM Tris HCl pH8. Sequencing was performed on an Illumina HiSeq 2500 machine (50bp read length, paired-end) or on an Illumina NextSeq 500 (75bp or 150bp read length, paired-end).

Sample preparation and 4C-Seq

4C assays using wild-type brainstem tissue were performed as described previously[38] with minor modifications. Two million of dissociated cells were cross-linked for 10 minutes with 2% paraformaldehyde, quenched with glycine and lysed in 50 ml lysis buffer (10mM Tris pH 7.5, 10mM NaCl, 2% NP-40, 1X protease inhibitors) for 30 minutes. Nuclei were then digested with

800U NlaIII enzyme (NEB, R0125) followed by 8 hours 'in nuclei' ligation at 16˚ C with 2000U T4 DNA Ligase (NEB, M0202) [39]. Reverse crosslinked and purified DNA was further digested with 50U DpnII enzyme (NEB, R0543), followed by circularization. 3200ng of 4C library was amplified with bait-specific inverse primers (read and amplification primers), pooled and purified. Amplified library was adaptor ligated, PCR amplified (8 cycles) and paired-end sequenced on the Illumina NextSeq 500 to obtain 75bp long reads. Read and amplification primers are listed in Supplementary Table 5.

Reverse transcription-PCR (RT-PCR) and quantitative-PCR (qPCR)

RT-PCR was done by SuperScript III Reverse Transcriptase (Thermo Fisher, 18080093) according to manufacturer's protocol. Oligo $d(T)_{18}$ mRNA primer (Thermo Fisher, SO131), 10mM dNTP Mix (Thermo Fisher, R0191) and RNase inhibitor (Promega, N2111) were used. qPCR was done using StepOnePlus Real-Time PCR System (Thermo Fisher) with SYBR Green PCR Master Mix (Thermo Fisher, 4309155) according to manufacturer's protocol using primers listed in Supplementary Table 5.

Quantification of *Fos, Egr1, Arc, Klf4, Junb* and *Gapdh* was done by ΔΔCt using *Actb* as an internal control, while the quantification of *Actb* (Extended Data Fig. 9e) was done using *Gapdh* as an internal control. A statistical analysis was performed by Welch's two-sample two-sided *t*-tests or by one-way analysis of variance (ANOVA) followed by Tukey's honest significant difference (HSD) post-hoc tests.

ChIP-qPCR

Embryonic hindbrain neurons were cross-linked with 1% formaldehyde in PBS 1X for 10 minutes at room temperature (RT) and quenched with 125mM glycine for 5 minutes at RT. Cells were rinsed twice with PBS 1X/ FCS 4%. Normally we prepared at least three biological replicates with 1,000,000 cultured neurons. Cells were lysed in 100 µl of Sonication Buffer (10mM Tris HCl pH8, 5mM EDTA, 0.15% SDS, 0.1X PBS, 1X Protease Inhibitor Cocktail) for 15 min on ice, and sonicated using the Covaris machine or the Bioruptor Pico machine to obtain DNA fragment the size of which distributes between 150bp and 500bp. After centrifugation (1 min, 10,000rpm, 4°C), the supernatant was transferred to new tubes, diluted four times with Equilibration Buffer. Chromatin solutions were incubated over-night at 4°C with 1µg of anti-H3K27me3 or anti-

H3K27ac antibodies. The next day, 40 µl of protein G coupled to magnetic beads were added and the incubation was continued for 2 hours at 4°C. The beads were then washed twice with RIPA Buffer and once with TE Buffer. DNA was eluted from the beads with 100 µl Elution Buffer at 65°C for 5hours. DNA was purified with SPRI AMPure XP beads (sample to beads ratio 1:2) and eluted in 60µl 10mM Tris HCl pH8. 4 µl of each sample was used for qPCR reaction. qPCR was done using StepOnePlus Real-Time PCR System with SYBR Green PCR Master Mix according to manufacturer's protocol using primers listed in Supplementary Table 5.
Quantification of *Fos* and *Egr1* was done by ΔΔCt using *Actb* or *Oct4* as an internal control. A statistical analysis was performed by Welch's two-sample two-sided *t*-tests or by one-way ANOVA followed by Tukey's HSD post-hoc tests.

ATAC-qPCR

ATAC-qPCR[40] experiments were performed as described previously with minor modifications. For each experiment, six independent biological replicates were used. Dissociated ESCs were collected into ice cold PBS 1X, and immediately pelleted by centrifugation (500 rcf, 5 minutes, 4°C). 20,000 cells were used for each experiment. Cells were washed once with 50µl PBS 1X and pelleted (500 rcf, 5 minutes, 4°C), and gently resuspended by pipetting in ice cold 50µl cold lysis buffer to extract nuclei and pelleted (500 rcf, 10 minutes, 4°C). Then nuclei were tagmented in transposition reaction mix (1 µl Tn5 Transposase (Illumina, FC-121-1030), 15µl 2X TD Buffer (Illumina, FC-121-1030), and 14µl nuclease free water) at 37°C for 30 minutes. DNA was purified with MinElute PCR Purification Kit by 10µl 10mM Tris HCl pH8. Library amplification was started with 1X KAPA HiFi HotStart Ready Mix, 1.25µl primers in total volume 50µl: 72°C for 5min; 98°C for 1min;11 cycles of 98°C for 15sec, 63°C for 30sec, 72°C for 1min. DNA was purified with SPRI AMPure XP beads (Beckman, sample to beads ratio 1:2) and eluted in 60µl 10mM Tris HCl pH8. 4 µl of each sample was used for qPCR reaction. qPCR was done using StepOnePlus Real-Time PCR System with SYBR Green PCR Master Mix according to manufacturer's protocol using primers listed in Supplementary Table 5. Quantification of *Fos* and *Egr1* was done by ΔΔCt using *Actb* as an internal control. A statistical analysis was performed by Welch's two-sample two-sided *t*-tests.

Plasmid construction

dCas9 over-expression vector (control vector, pEF1a_dCas9) was constructed from dCAS9-VP64_GFP plasmid by removing the *VP64* sequence. dCAS9-VP64_GFP was a gift from Feng Zhang (Addgene Plasmid #61422)[41]. Subsequently, dCas9-UTX fusion protein over-expression vector (pEF1a_dCas9-UTX) was generated by inserting the CDS of mouse *UTX* to the 3' of *dCas9*. Guide RNA (gRNA) over-expression vector (pGuide_EGFP) was constructed by replacing the *hSpCas9* sequence of pX330-U6-Chimeric_BB-CBh-hSpCas9 plasmid with the *EGFP* sequence. pX330-U6-Chimeric_BB-CBh-hSpCas9 plasmid was a gift from Feng Zhang (Addgene Plasmid #42230)[42]. Two gRNAs targeting the gene body regions of mouse *Fos*, *Egr1*, *Gapdh*, and *Actb* gene loci are designed and inserted into the BpiI (Thermo Fisher, ER1011) cut site of pGuide_EGFP. Inserted sequences are following. Targeted sequences are listed in Supplementary Table 5.

TVA/EnvA trans-synaptic tracing and PrV neuron dendrite analysis

EnvA-pseudotyped G-deleted rabies viruses (*EnvA-SAD-ΔG-Rabies:EGFP* virus[43]) were stereotaxically injected (Kopf Instruments) into P3 wild-type $K20^{TVA/+}$ or barrelette neuron activity-deprived $K20^{TVA/Kir}$ VPM (from Bregma: 1.2 mm posterior, 1.0 mm lateral, and 2.4 mm ventral). A small craniotomy was performed and a pulled-glass pipettes were used for local infusion of the virus by multiple short pulses using a picospritzer (Parker). To trace vPrV barrelette and for the transsynaptic experiments neurons mice were sacrificed 7 days later (P10), perfused with 4% PFA, and 60-µm vibratome brain sections collected. To trace vPrV barrelette at least 5 neurons were analysed for each mouse (for $K20^{TVA/+}$ and $K20^{TVA/Kir}$ conditions). Confocal imaging was performed with 40× objective (Zeiss LSM700 microscope). Arbors were traced using ImageJ neurite tracer software.

Matlab ad-hoc code was created in order to calculate the symmetric index and the surface ratio. Neurons were divided in the two half spheres by a rotating plane (5 degrees steps). Dendrites density was calculated in both half spheres and the ratio among the two densities (numerator as lower term and denominator as the highest) was calculated for each step of the plane. In the Extended Data Fig. 1n, o, example of the ratio on each plane calculated for a $K20^{TVA/+}$ (n) and $K20^{TVA/Kir}$ (o) barrelette neuron is shown by the color codes (percentage of the lower dendritic density over the higher dendritic density). The lower point (zero in case of total asymmetry) was defined as the Symmetric Index. Surface Ratio describes the probability that the plane will be

settled in a point of the function having a Symmetric index equal to zero. Statistical analysis was performed by Welch's two-sample two-sided *t*-tests on the averages of the Symmetry indexes and Surface Ratios calculated from different cells in the same animals.

3D reconstruction and nuclei volume calculation

Volumes of PrV were calculated upon a 2.5D reconstruction. Coronal vibratome sections (60 µm) of the PrV from P8 pups $K20^{tdTomato/+};r2^{EGFP/+}$ or $K20^{Kir/+};r2^{EGFP/+}$ animals were collected. Imaging was performed using a confocal microscope (Zeiss LSM700). 2.5 D reconstructions were made using Fiji/ImageJ and volumes were calculated upon processing with Imaris® software selecting the corresponding color. A threshold was imposed in order to eliminate small dots and background. A statistical analysis was performed by Welch's two-sample two-sided *t*-tests.

Histological analysis

Postnatal brains were perfused, dissected and also left overnight in 4%PFA. Sections were obtained upon vibratome cut (60 µm). Sections were incubated overnight at 4°C with primary antibodies anti-GFP (1:500, Abcam, ab290, PRID: AB_303395) or anti-RFP (1:1,000, chromotek, 5f8-20), rinsed three times in PBS and incubated for 60–90 min at room temperature with Alexa Fluor 488- and/or 546- and/or 647 conjugated secondary antibodies (1:1,000, Invitrogen, A11034, PRID: AB_2576217, A21245, PRID: AB_2535813, A11077, PRID: AB_2534121). Nuclei were stained with DAPI (ThermoFisher, D1306). Cytocrome oxydase staining was performed as previously described[1].

Reference genome and annotation

The mouse GRCm38/mm10 genome assembly was used as a reference and the analyses were done using R (https://www.r-project.org, versions 3.5.1 and 3.5.3).

TSS selection:

Transcription start sites (TSS) were obtained from the *TxDb.Mmusculus.UCSC.mm10.knownGene* Bioconductor package (https://doi.org/doi:10.18129/B9.bioc.TxDb.Mmusculus.UCSC.mm10.knownGene, version 3.4.0), and in the case of multiple TSSs per gene the one with the highest variance in chromatin accessibility (ATAC-seq, window of 2kb centered on TSS) was chosen. For this, ATAC-seq reads

were counted using *qCount* from *QuasR* [44](version 1.22.1) for the E10.5 progenitor, and E14.5, E18.5, and P4 barrelette (vPrV) samples. The raw counts were normalized using calculated scaling factors as follows: For each sample, ATAC peaks were called using MACS2 [45](version 2.1.1.20160309) with options *–f BED*, *--nomodel*, *--shift -100*, *--extsize 200*, and *--keep-dup all*. For each sample, the number of reads per base (rpb_{sample}) was calculated by dividing the sum of reads outside called peaks by the non-peak genome (autosomes only). The scaling factor (sf) was calculated as sf_{sample} = min(rpb of all samples)/rpb_{sample}. The corrected counts were log2-transformed with a pseudo-count of 8. For each gene, the TSS with the highest variance in accessibility across all conditions was selected. If multiple TSSs shared equally high variance, a random TSS was chosen. Only autosomal genes were considered. Choosing the TSS in other ways gave similar results. Namely, selecting the TSS that has the maximum ATAC signal per gene resulted in a set of TSSs similar to the previous one. Excluding genes where the TSS was randomly chosen, the TSS overlap between the two methods was 94.6%.

Promoter and gene body regions:

Promoter (P) regions were defined as 1000bp upstream and 500bp downstream of the chosen TSS per gene. Gene Body (GB) regions were defined as the region between 1001 bp and 3000 bp downstream the chosen TSS, giving GBs a maximum width of 2 kb (green and blue rectangles in Extended Data Fig. 5a). This definition also left a gap of 500 bp between promoter and gene body regions in order to prevent any overlap of signals between them. Genes with overlapping promoter or gene body regions, as well as genes that were too short were excluded.

Transcription end site:

The transcription end sites (TES) were defined for genes in the P and GB sets as the last 2kb of the transcript with the most downstream transcript end site from all transcripts of each gene.

Salmon spliced and unspliced transcript indexing:

Spliced transcripts were obtained from the *GENCODE*[46] vM19 transcriptome fasta file (ftp://ftp.ebi.ac.uk/pub/databases/gencode/Gencode_mouse/release_M19/gencode.vM19.transcripts.fa.gz), and for each transcript, the corresponding unspliced version was created as the full sequence from the first exon to the last (including all introns and exons in between). Sequence-duplicated spliced transcripts and short spliced transcripts (less than 31 bp) along with their corresponding unspliced forms were removed. *Salmon* [47](version 0.12.0) was used to build a quasi mapping index on the fasta file with *–k 31*.

Read alignment to the reference genome

mRNA-seq (SmartSeq2):

Reads were aligned to the reference genome with *STAR* [48](version 2.5.2b) using parameter values similar to the ones suggested by *ENCODE* with options *--outFilterType BySJout*, *--outFilterMultimapNmax 20*, *--outMultimapperOrder Random*, *--alignSJoverhangMin 8*, *--alignSJDBoverhangMin 1*, *--outFilterMismatchNmax 999*, *--alignIntronMin 20*, *--alignIntronMax 1000000*, and *--alignMatesGapMax 1000000,* and converted to bam files with *samtools* [49](version 1.2).

Total RNA-seq (Ovation SoLo RNA-Seq):

Reads were trimmed for the GATCGGAAGAGCACACGTCTGAACTCCAGTCAC adapter from the 3' end with *cutadapt*[50] (version 1.15) using *overlap=1*. Trimmed reads were mapped to the reference genome using *STAR* (version 2.5.2b, using identical parameters as above for the SmartSeq2 data) and *samtools* (version 1.2). In addition, for the E14.5 *Drg11*$^{vPrV\text{-}ZsGreen/+}$, E14.5 *K20*$^{tdTomato/+}$ and E14.5 *Ezh2cKO*$^{r3\text{-}RFP}$ samples, reads were used to estimate spliced and unspliced transcript abundances per gene with *salmon* (version 0.12.0) with the parameters *--validateMappings*, *--fldMean 350, --seqBias*, and *--gcBias*. For downstream analyses, transcript abundances were combined to obtain gene abundances (see below).

ATAC-seq:

For better comparability with 51-mer paired-end (PE) samples, the samples that had been sequenced as 76-mer PE reads were trimmed to 51-mer PE reads by removing the last 25 bp using *cutadapt* (version 1.12 and 1.18). In addition, the adapter sequence CTGTCTCTTATACACA was trimmed from the 3' end of all samples with *overlap=1*. The trimmed reads were aligned with *bowtie2*[51] (version 2.3.0 and 2.3.4.2) with the options *--fr*, *--minins 0*, *--maxins 1000*, *--no-discordant* and *--dovetail*, and converted to bam files using *samtools* (version 1.2 and 1.9).

ChIP-seq:

The ChIP-seq samples that were prepared by the ChIPmentation protocol were trimmed for the adapter sequence CTGTCTCTTATACACA from the 3' end using *cutadapt* (versions 1.15 and 1.18) with *overlap=1*. The ChIP-seq samples prepared by NEBNext Ultra DNA Library Prep Kit (i.e. E12.5 short-term cultured hindbrain neurons that were treated by DMSO (control) or TSA, see above) were trimmed using *cutadapt* (version 1.15) for the

GATCGGAAGAGCACACGTCTGAACTCCAGTCAC adapter from the 5' and then the 3' ends since the adapter was seen on both ends during visual inspection of the fastq files. The trimmed reads were mapped to the reference genome using *bowtie2* (versions 2.3.3.1 and 2.3.4.2) and converted to bam files using *samtools* (versions 1.6 and 1.9).

The ChIP-seq samples from the public datasets were processed in the same way, but differed at the adapter trimming step. For the mouse embryonic and adult cortex ChIP-seq (GSE93011 and GSE52386, GSE63137), reads were trimmed for the GATCGGAAGAGCACACGTCTGAACTCCAGTCAC adapter from the 5' end. The cultured embryonic cortical neuron ChIP-seq (GSE21161) was mapped to the reference genome using *bowtie*[52] (version 1.0.0) with the *–C* option to allow for colorspace alignment. For the public ESC dataset (GSE36114 and GSE94250), the adapter (GATCGGAAGAGCACACGTCTGAACTCCAGTCAC) was trimmed on both the 5' and 3' ends, while it was trimmed from the 5' end for the dataset from Lavarone et al.,[22] (GSE116603).

4C-seq:

Coordinates of expected 4C fragments were created by *in silico* digesting the reference genome with restriction enzyme one (DpnII). Valid fragments were defined as non-blind fragments (containing a site for restriction enzyme two (NlaIII)) where the distance between the fragment start/end to the first/last site for restriction enzyme two was greater than 30bp. Reads were aligned to the genome with *QuasR* (version 1.22.1) using *qAlign* with default parameters. Sample quality was assessed using the criteria (percent of covered fragment ends 0.2 Mb around viewpoint and percent of reads in cis) described in [53]. Reads were counted per fragment using *qCount* from the *QuasR* package, normalized by dividing by the number of aligned reads in a sample on the cis chromosome (the chromosome containing the viewpoint) and multiplying with 1e6 (counts per million cis-chromosome alignments) and exported as a bedGraph file for visualization using *rtracklayer*[54] (version 1.42.2). For visualization of combined replicates, normalized fragment counts were averaged across replicates and smoothed using a running mean over three adjacent fragments.

BigWig Files:

For genome browser views, the number of alignments per 100 bp window in the genome and per million alignments in each sample were calculated and stored in BigWig format with *QuasR* (version 1.22.1) using the *qExportWig* function with *binsize=100* and *createBigWig=TRUE.* The

autosomal library size was used to normalize for library size differences across samples, since each sample was a mixture of mouse embryos of different sexes (this was achieved by setting *scaling* = autosomal library / full library size * 1e6, which will cancel out the full library size normalization the function does internally). Counts per bin were averaged across replicates to create BigWig files that represented a single condition. For the ATAC-seq data, *pairedAsSingle=TRUE* option was used in order to create a wig file of fragment cut sites, instead of fragment mid points.

For a subset of samples, normalized BigWig files were created in order to reduce between-sample non-linearities as follows: For the ATAC-seq, H3K27me3, H3K4me2, and H3k27ac of the samples from E10.5 progenitors, E14.5vPrV, E18.5vPrV, and P4vPrV, initial BigWig files were created setting *scaling* equal to the total mapped reads (so that it cancels out the normalization in the function). The same kind of normalization was done for the RNAPII-S2P, RNAPII-S7P, and H3K36me3 samples at E14.5, E18.5 and P4. For each chromatin mark, counts from the resulting BigWig files were read into *R* and *limma's normalizeCyclicLoess*[55] (version 3.38.3) function was used on the log2-transformed counts per bin with *method="fast"*. This normalization corrected for differences in library size and other non-linearities between different samples. The corrected counts were transformed back from the log2 to the raw count space and exported as normalized BigWig files. These normalized BigWig files were scaled to the counts per million (CPM) level afterwards. Counts per bin were averaged across replicates to create BigWig files that represented a single condition.

To visualize the BigWig files for replicates of H3K27me3 ChIP-seq of the dCas9 or dCas9-UTX over-expressed cultured hindbrain neurons on top of each other (see Extended Data Fig. 9b), the *plotCoverage* function from the *wiggleplotr*[56] package (version 1.6.1) was used with the options *mean_only = FALSE*, *alpha=0.5*, *flanking_length = c(200,200)* and *rescale_introns = FALSE*.

Read quantification and abundance estimation

RNA-seq:

Reads were quantified for genes from the *TxDb.Mmusculus.UCSC.mm10.knownGene* Bioconductor package (https://doi.org/doi:10.18129/B9.bioc.TxDb.Mmusculus.UCSC.mm10.knownGene, version 3.4.0) and *QuasR*'s *qCount* function with *mapqMin=11* and *mapqMax=255*. Only autosomal

genes were kept since the samples consisted of mixtures of embryos of different sexes. Reads per kilobase million (RPKM) were then calculated, averaged across replicates, and log2-transformed with a pseudo-count of 0.1.

For samples whose transcript abundance was quantified with *salmon*, the *tximport* function from the *tximport*[57] (version 1.10.1) package was used to get the abundance matrix which contains the spliced and unspliced transcript per million (TPM) counts for each gene and sample. The TPMs were log2-transformed with a pseudo-count of 1.

Single Cell RNA-seq:

The single-cell RNA-seq data was quantified with *CellRanger*[58] (version 3.0.2), using a reference transcriptome generated from the mouse mm10 genome and the Gencode (version M20) genome annotation. Quantifications were imported into R (version 3.6.1) using the *DropletUtils* package[59] (version 1.4.3), quality control was performed using *scater*[60] (version 1.12.2), and normalization and log-transformation of UMI counts with *scran*[61] (version 1.12.1) and *scater*. Cells with total UMI count below 6,500 (E10.5) or 3,500 (E14.5) were excluded from further analyses. The remaining 2,646 cells from E10.5 had a median UMI count of 12,419 (range 6,502-47,172), and the median number of detected genes was 4,070 (range 2,454-7,739). The 2,513 retained cells from E14.5 had a median UMI count of 6,339 (range 3,505-21,288), and the median number of detected genes was 2,922 (range 1,836-5,847). A gene was considered 'observed' in a cell if the UMI count was greater than 0.

ATAC-seq and ChIP-seq:

Reads were quantified on the defined regions using *qCount* from *QuasR* (version 1.22.1). For H3.3, Cdk9, Ring1b and 8WG16 RNAPII, RPKMs were calculated using the read count sum on the P and GB as the library size per sample, averaged across replicates and finally log2-transformed with a pseudo-count of 0.1. In calculating RPKMs on the P region for S5P RNAPII and S7P RNAPII the library size was the read count sum on the P regions. The RPKMs for S2P RNAPII and H3K36me3 on the TES were calculated using the read count sum on the TES regions as the library size (Fig. 4a, b).

For the H3K27me3 ChIP-seq from the dCas9 experiments, the counts per million (CPM) on the GB regions were calculated, averaged across replicates, and log2-transformed with a pseudo-count of 8. From the MA plot shown in Extended Data Fig. 9d, a set of genes (green) that have similar average log2-transformed CPM (logCPM) as the Fos gene (red) were selected by

taking all genes +/- 0.5 logCPM of the Fos gene logCPM (1081 genes selected), in order to compare the Fos gene against a group of genes that have similar levels of H3K27me3. The median of the E14.5Bip genes' log2-fold change (logFC) that fall in this region of the MA plot was calculated as well (Extended Data Fig. 9d). The percentages of genes within the selected groups, that have a logFC value less than or equal to that of Fos (1.48%) or the median E14.5Bip genes (which fall in the green region) (45.24%) were calculated.

The Jmjd3 ChIPs were analyzed by quantifying reads on the defined P and GB regions. The sum of reads on P and GB was used as library size per sample, and used when calculating counts per million (CPM) across the genes. The CPMs on the GB regions were averaged across replicates, log2-transformed with a pseudo-count of 8, and used to create the MA plot in Fig. 7e, highlighting E14Bip genes that gain expression at P4 (RPKM > 3 at P4).

The pCREB ChIP-seq reads for E14.5 and P4 (see Fig. 7a) were quantified on the promoters, corrected for library size differences using the total mapped reads, and log2-transformed with a pseudo-count of 1. These were then used to calculate log-fold changes (logFC) between the P4 and E14.5 samples (logFC P4/E14.5). More detailed analyses of other ChIP-seq datasets that required specific normalizations are described below.

Visualizing combined chromatin states with t-SNE

The H3K27me3, H3K27ac, and H3K4me2 marks as well as chromatin accessibility (ATAC) were quantified for each gene in P and GB regions using the *qCount* function from *QuasR* (version 1.22.1). RPKMs were calculated using the sum of the total P and GB counts as the library size per sample. RPKMs were averaged across replicates and log2-transformed with a pseudo-count of 0.1 to obtain a matrix with genes as rows and the log2-RPKMs in P and GB regions of the mentioned chromatin marks as columns. t-Distributed stochastic neighbor embedding (t-SNE)[62] was used to create a 2-dimensional embedding of this matrix, placing genes with similar chromatin landscapes close together.

For the E14.5, E18.5 and P4 samples, an additional normalization step was performed to reduce non-linearities between samples and therefore improve comparability, using *limma's* (version 3.38.3) *normalizeCyclicLoess* with *method="fast"*. A t-SNE embedding was then calculated on the corrected counts using *Rtsne* (version 0.13).

Bipartite and bivalent scores:

To calculate a 'bipartiteness' score for genes, we selected genes that had low expression (RPKM < 3), greater levels of H3K27ac in P than in GB, and greater levels of H3K27me3 in GB than in P. The selected genes' H3K27ac in P and H3K27me3 in GB were ranked separately from low to high, and the two ranks for each gene were summed up.

A 'bivalency' score was calculated for genes that also had low expression values (RPKM < 3). H3K27me3 in P and H3K4me2 in P were ranked from low to high, and the two ranks for each gene were and summed up. Genes that were high in both marks thus got high 'bivalency' scores.

Both scores were evaluated separately for each time point by selecting the top 100 high-scoring genes and about 300 additional genes selected from a broad range of scores, and inspecting the distribution and levels of histone marks in a genome browser (e.g. to evaluate the E14.5 barrelette neuron profile, the first top 100 bipartiteness scoring genes were all visually inspected one by one whereas from 101-500 we randomly chose sets of 20 genes every 40-100 in the list for visual inspection). Inspected genes were manually classified into bipartite (high H3K27ac in P, high H3K27me3 in GB) or bivalent (both high H3K27me3 and H3K4me2 in P) in order to calculate the fraction of true positives at any given score (Extended Data Fig. 3a, b). For every developmental time point, a function was fitted on the true positive fraction versus the top scoring genes using the *interpSpline* function with *bSpline=TRUE* from the *splines*[63] R package. Producing the bipartite and bivalent scores using 2 biological replicates of the ChIP-seqs gave highly similar scores across genes between the 2 replicates and a pearson correlation of 0.91 and 0.93 for the bipartite and bivalent scores, respectively, between the two replicate scores.

The total number of bipartite and bivalent genes in each time point was then estimated as the area under the curve (AUC) of the fitted splines. The same steps were done to obtain bipartiteness and bivalency scores for genes using the public datasets for mouse ESCs, our own ESC datasets, E10.5 NCCs and E14.5 liver and heart tissues (Fig. 2a). To inspect the intersection of the top 100 bipartite genes from the different tissues, the *upset* function from the *UpSetR* package[64] (version 1.3.3) was used with *order.by="freq"* (see Fig. 2d).

Bipartite and bivalent regions on t-SNE:

Using the 100 top-scoring genes for the single time point t-SNE (E10.5 t-SNE) map and the top 300 genes for the combined t-SNE map (E14.5/E18.5/P4 combined t-SNE), two-dimensional densities for bipartite and bivalent genes were estimated with the *kde2d* function from the *MASS*[65]

(7.3.51.1) package using a grid size of 25, and shown as the contour lines on the t-SNE plots (see Extended Data Fig. 5g, l).

Chromatin profiles of top 100 bipartite and bivalent genes:

The chromatin mark distribution surrounding the selected TSSs (2.5 kb upstream and 6 kb downstream) for the top 100 bipartite and top 100 bivalent genes in E14.5 barrelette, ESCs, E10.5 NCCs, E14.5 mouse liver and E14.5 mouse heart tissues were obtained using *QuasR*'s *qProfile* (version 1.22.1) function (see Fig. 2b). The counts were corrected for library size differences by multiplying the counts by scaling factors (sf) that were obtained using the total number of reads mapped on the autosomal genome as the library size per sample: sf_{sample} = min(lib size) / sample-specific lib size. The corrected counts were averaged per condition and chromatin mark and smoothed with the *runmean* function with *endrule="constant"* and using *k=601* for the E10.5 NCC and *k=801* for the rest.

For visualization, chromatin mark profiles were scaled to the interval [0,1] for easier comparison as follows: For each mark, we chose a minimum (min) value that was the median of the counts on the first and last 500 bp (-2.5kb to -2kb, and 5.5kb to 6kb relative to the TSS) and a maximum (max) value that was the maximum count in both the bipartite and bivalent profiles to also make the two profiles comparable to each other after the scaling. For each mark, the min value was then subtracted from the profile and the result was divided by (max-min) resulting in a scaled count between 0 and 1 (scaled count = (raw count - min) / (max - min)).

Chromatin dynamics in the t-SNE:

We calculated Euclidean distances of genes between P4 and E14.5 on the original 8-dimentional space consisting of normalized log2(RPKM) counts of ATAC, H3K27me3, H3K27ac, and H3K4me2 on the P and GB regions, and colored the E14.5 t-SNE by this distance (see Extended Data Fig. 5h). To further explore the properties of the E14.5Bip genes across development, they were divided into 3 groups: E14.5Bip genes that become expressed at P4 (RPKM >=3 at P4), that become bivalent (selected by taking the genes that move into the red bivalent contour on the t-SNE at P4, see Fig. 3d), and that remain bipartite (the remaining E14.5Bip genes) (see Extended Data Fig. 6a).

Selection of genes to compare to E14.5Bip Genes

Groups in Fig. 4:

We first selected the top 100 bipartite genes at E14.5 (E14.5Bip genes, using the 'bipartiteness' score) and the top 100 bivalent genes at E14.5 (E14.5Biv genes, using the 'bivalency' score) and excluded 3 genes that were found in both sets, leaving two distinct sets of 97 E14.5Bip and 97 E14.5Biv genes. Several control sets of the same number of genes (97) were then created as follows: E14.5AcP genes were sampled from all genes except for the top 400 E14.5 bipartite genes and E14.5Biv genes to have similar H3K27ac distribution in P as the E14.5Bip genes, using the *sampleControlElements* function from the *swissknife* package (https://github.com/fmicompbio/swissknife, version 0.10). E14.5mRNALow genes that match the E14.5Bip genes in log2-RPKM mRNA expression (smartSeq2) were sampled similarly from all genes except E14.5Biv genes, the top 400 E14.5 bipartite genes and E14.5AcP genes. Finally, two gene sets were sampled from the bottom and top 30% of genes ordered by mRNA expression, excluding any of the genes already contained in the previously defined groups.

Genes in Extended Data Fig. 7a, b:

Entrez identifiers from the top 100 E14.5Bip genes were first mapped to their corresponding Ensemble IDs using the *useMart* function from *biomaRt*[66] (version 2.38.0) with the options *biomart="ensembl"* and *dataset="mmusculus_gene_ensembl"*, resulting in a set of 90 successfully mapped E14.5Bip genes. A control set of 90 genes matching the E14.5Bip genes in spliced transcript abundance (in the log2(average TPM + 1)) and not in the top 400 E14.5 bipartite genes was then randomly sampled as described above. Genes with zero total counts were excluded (between 0 and 14 genes per replicate and gene set).

Ezh2cKO analyses (E14.5)

H3K27ac and H3K27me3 ChIP-seq (Fig. 5a):

The knock-out of *Ezh2* caused genome-wide changes in histone modification levels and thus the total number of alignments cannot be used as a library size proxy for normalization. To normalize these samples for differences in library size, we therefore selected a group of genes that were constantly expressed, assuming that the promoter regions of these genes are likely to not exhibit changes in chromatin marks between the two conditions. We selected genes that had an absolute logFC of less than 0.2 between the wt and *Ezh2cKO* and an average logCPM >= 5 based on differential expression analysis with *edgeR*[67] (version 3.24.3). We further excluded from our selection of control genes the genes that overlapped with any of the Polycomb regions on our t-

SNE maps (including the bipartite and bivalent regions), resulting in a total of 1,166 genes. Promoter (as defined in the previous sections: -1kb and +500bp relative to the selected TSS per gene) reads of the selected genes were summed for each sample *i* (N_i) and used to calculate scaling factors for sample $i = \min(N_i)/ N_i$ .These scaling factors were then multiplied by the raw counts in each sample, and corrected counts were then averaged across replicates and log2-transformed with a pseudo-count of 1.

SmartSeq2 MA Plot (Fig. 5b):

The CPMs of the autosomal genes were calculated, averaged across replicates, and log2-transformed with a pseudo-count of 8. The logFC (M values) and average logCPM (A values) were calculated and E14.5Bip genes were shown in red.

E14.5 vPrV fraction of TSS proximal reads (Fig. 5c):

To calculate the fraction of reads at the beginning of each gene, we used the selected TSS for each gene as described above. The beginning of the gene was defined as 200 bp downstream and 100 bp upstream of the TSS, including only exonic regions. Reads were then counted in this region for each gene and normalized by calculating CPMs using the same library size as for the normalization of the whole gene counts. Replicate CPMs were averaged, and only genes with a CPM of at least 1 in both the wt and *Ezh2cKO* were kept (of the E14.5Bip genes, 82 out of 100 remained). For visualization, the log2 ratio compared to the whole genes was calculated as $\log2((CPM_{beginning} + 1)/(CPM_{whole} + 1))$.

Total RNA (SoloSeq) Spliced and Unspliced Transcript Abundance:

We used the total RNA-seq dataset to look at differences in spliced and unspliced transcript abundances between the wt and *Ezh2cKO* on genes that had a TPM of at least 0.05 in both their spliced and unspliced forms in at least 1 sample. For each of the two conditions, the fraction of transcripts in the spliced form was calculated as (TPM spliced) / (TPM spliced + TPM unspliced) (Extended Data Fig. 7c).

ATAC Ezh2cKO vs Ctrl (Fig. 5d and Extended Data Fig. 8b):

E14.5 and P4 barrelette enhancers were defined using the peaks called on each condition with the ATAC-seq. The defined peaks were combined for both conditions, and only distal (at least 1kb away from any TSS) and autosomal peaks were kept and used as our set of enhancers. ATAC-seq for the *Ezh2cKO* and ctrl samples, as well as the E14.5 and P4 samples were quantified on the defined enhancers. The counts were log2-transformed with a pseudo-count of 1, underwent

normalization with the *normalizeCyclicLoess* function from *limma*, and were averaged across replicates. Using the bed files from Malik et al., 2014[14], we used the union of the two KCl-treated Fos ChIP bed files to define neuronal activity-dependent Fos targets, and divided our enhancers into Fos-overlapping (enhancer overlapping Fos target) and non-Fos-overlapping (enhancers not overlapping Fos targerts). We focused our analysis on enhancers that show an ATAC log-fold change greater than 1.5 from E14.5 to P4: 85 Fos-overlapping enhancers, and 3,882 non-Fos-overlapping enhancers, and looking at their *Ezh2cKO* vs ctrl ATAC logFC.

H3K36me3 Ezh2cKO vs WT (Extended Data Fig. 7e):

Reads were quantified on the full selected transcript per gene, and RPKMs were calculated followed by a log2-tranformation with a pseudo-count of 1. In each condition, we used the *Mclust* function from the *mclust* package[68] (verison 5.4.3) with *G=2* and *modelNames="V"* to fit a two-component Gaussian-mixture model to the log2-RPKMs, and used the fitted distributions to define a threshold value for a specific mark corresponding to an FDR of 0.05 (dashed green lines in Extended Data Fig. 7e) as described in Minoux et al., 2017[69].

Sequential ChIP analysis

Reads were quantified on joint P and GB regions, defined as the start of P to the end of GB. CPMs were calculated and averaged across replicates. Genes with low mappability (less than 80% mappable positions for 50-mer reads in joint P and GB regions) were removed. H3K27me3 was plotted against H3K27ac and colored by the sequential ChIP (Extended Data Fig. 4b). The sequential ChIP signal (color gradient) increases both in the directions of the x and y axes, indicating that the sequential ChIP was successful and that the two histone modifications co-exist on individual chromatin fragments.

We used the *Mclust* function from the *mclust* package[68] (verison 5.4.3) with *G=2* and *modelNames="V"* to fit a two-component Gaussian-mixture model to the log2-counts of each ChIP mark, and used the fitted distributions to define a threshold value for a specific mark corresponding to an FDR of 0.05 (dashed green lines in Extended Data Fig. 4b) as described in Minoux et al., 2017[69].

Defining activity response genes (ARGs)

bsARGs:

barrelette sensory ARGs (bsARGs) were defined using the mRNA samples of E14.5 vPrV, E18.5 vPrV, and E18.5 vPrV Kir-OE barrelette neurons. Only autosomal genes were considered and differential expression analyses were done with *edgeR* (version 3.24.3). The model was fit with *glmQLFit* using all the mRNA samples from E10 to P4 WT and Kir-OE on genes that have a CPM > 1 in at least 2 samples. Genes that were not or only lowly expressed at E14.5 (RPKM < 3) and that were upregulated from E14.5 to E18.5 WT were selected using a logFC >= 1.5 and a logCPM >= 2 (n = 702) (Extended Data Fig. 1q). Genes that were not or only lowly expressed at E14.5 (RPKM < 3) and that were downregulated between E18.5 vPrvKir-OE and E18.5 vPrV WT were selected as having a logFC <= -1 and a logCPM >= 2 (n = 102) (Extended Data Fig. 1r). The intersection of these two sets of genes (n = 56 genes) was taken as the bsARGs (Extended Data Fig. 1q-s). The barplot in Fig. 1c compared the bsARGs to all other genes that were also not expressed at E14.5. A gene was Polycomb-overlapping if any of its transcripts overlapped with the defined Polycomb regions using *findOverlaps* from GenomicRanges (version 1.34.0).

nbARGs:

Non-barrelette ARGs (nbARGs) were defined based on the literature[9-11] using the ARGs as described in the public datasets section. All activity-dependent genes (rapid and late induced genes) were used and only the genes that are not expressed (RPKM < 3) in all of E14.5, E18.5 and P4 in the barrelette neurons and do not overlap with the bsARGs were kept (83 genes). In the barplot (Fig. 1c) they were compared to all other genes that are not ARGs from the 3 papers, nor bsARGs, and also not expressed at any of the three developmental time points (RPKM < 3).

ATAC and H3K4me2 of bsARGs and nbARGs (Extended Data Fig. 1u):

All autosomal TSSs were obtained using the *transcripts* function with the *TxDb.Mmusculus.UCSC.mm10.knownGene* Bioconductor package (https://doi.org/doi:10.18129/B9.bioc.TxDb.Mmusculus.UCSC.mm10.knownGene, version 3.4.0) and the E14.5 vPrV ATAC-seq was quantified on all TSSs +/- 1kb. The TSS with the highest ATAC signal was chosen per gene, and if multiple TSSs had equally high values the selection was done randomly with the *sample* function. A 2 kb region (1 kb upstream and 1 kb downstream the selected TSS) was defined as a promoter region and the ATAC-seq and H3K4me2 were quantified on these regions with *qCount* from *QuasR* (version 1.22.1). CPMs per sample were calculated, averaged across replicates, and log2-transformed with a pseudo-count of 1.

To define the cutoff for being positive or negative for ATAC and H3K4me2, a two component Gaussian-mixture model was fit per mark on the log2-transformed counts using the *mclust* package[68] (version 5.4.1) and a threshold corresponding to an FDR of 0.05 was calculated as described in Minoux et al., 2017[69].

IEGs and LRGs (Fig. 1d):

A set of immediate early genes (IEGs) and a set of late response genes (LRGs) were obtained from the literature[9-11]. All bsARGs and nbARGs were considered and only the genes that are Polycomb-overlapping (a gene is considered to be Polycomb-overlapping if any one of its transcripts overlaps with the defined Polycomb regions as described in the section below), ATAC+ and H3K4me2+ (a gene is positive for ATAC or H3K4me2 if its count on the defined promoters described above was greater than the threshold derived with the set Gaussian-mixture model and FDR), and are rapid response genes in any of the papers were defined as IEGs (IEGs with RPKM < 3 at E14.5). The LRGs were the rest of the ARGs that are also polyc-overlapping, ATAC+, H3K4me2+, and non-IEGs (also with RPKM < 3 at E14.5). The IEGs and LRGs were viewed in the genome browser to manually classify them as bipartite or bivalent (in E14.5 vPrV).

Identifying E14.5 vPrV Polycomb domains

A hidden semi-marov model (HSMM) was used to identify Polycomb domains (chromatin that is positive for the H3K27me3 histone modification) genome-wide. This approach was used instead of typical peak callers since the size of Polycomb regions varies a lot across the genome, from short peaks up to large domains. A hidden markov model (HMM) or peak callers like *MACS2* will be unable to find optimal parameters that model both short and long regions and typically do not account for this variation. We therefore tiled the genome into 500 bp regions and the H3K27me3 ChIP-seq read count per tile was log2-transformed with a pseudo-count of 1. In an HMM setting these are the observations, and the hidden states that are to be inferred are “Polycomb” and “non-Polycomb”. The HSMM in addition models the duration of a state and thus was better suited to call Polycomb domains.

The *mhsmm*[70] (version 0.4.16) R package was used. The *hsmmspec* function was used to estimate the model parameters assuming a Gaussian distribution on the emissions (the log2-count data of the two states) and a gamma distribution on the sojourn (duration of a state). The *hsmmfit*

function then used the model's estimated parameters with *mstep=mstep.norm* and *maxit=100*, to call Polycomb and non-Polycomb regions.

TSA-treated cultured hindbrain neuron data

Quantifying and normalizing ChIP-seq counts on the gene body:

The control (DMSO-treated) and TSA-treated ChIP-seq (H3K27me3 and H3K27ac) samples had different log(raw cnt) vs percent GC trends (having quantified on 2kb tiles genome-wide). Left uncorrected, the logFC values between Ctrl and TSA-treated can be driven by differences in GC content. To correct for this, we first set out to define a reasonable set of background tiles (that are not positive for the marks). *MACS2* (version 2.1.2) was used to call peaks for each sample with the following parameters: *--nomodel*, *--extsize 100*, *--shift 0* and *--keep-dup all*. The background (non-signal) set of tiles were defined as those that do not overlap with any of the called peaks in any sample. The log2(raw cnt) vs percent GC trend was estimated with a linear fit for each sample on the defined background tiles (composing around 85% of all original tiles) using the *lm* function in R. These fits were used to correct the gene body counts (on the log2(raw counts + 8)). For each mark, the expected count for a given percent GC was calculated using the fits, and counts were corrected by setting one sample as the reference to which the trend of the other is pulled, by subtracting the difference in the expected values of the reference sample and the one being adjusted (delta), from the original count value: $\log2(\text{raw count adjusted})_{\text{sample}} = \log2(\text{raw count})_{\text{sample}} + \text{delta}_{\text{sample}}$, where $\text{delta}_{\text{sample}} = (\text{predicted reference sample count}) - (\text{predicted count})_{\text{sample}}$. In this manner, we corrected simultaneously for non-linearities in GC trends and library sizes using the fits on the background tiles. Where there were multiple replicates per condition, the corrected counts (which are in log2-space) were averaged per condition.

Fig. 7k:

The logFC values between TSA-treated and ctrl conditions on the gene body were calculated for H3K27me3 and H3K27ac using the corrected counts described above. For the mRNA, counts per million (CPM) were calculated on the autosomal genes, averaged across replicates, and log2-transformed with a pseudo-count of 1 to subsequently calculate logFC values. The E14.5Bip genes (top 100 bipartiteness ranked genes at E14.5 in barrelette neurons) are highlighted in Fig. 7k and colored by the mRNA (TSA/ctrl) logFC.

ESC *EedKO* analyses

Quantifying WT ChIP-seq:

The WT ESC levels of H3K27ac, H3K27me3 and H3K4me2 on the defined P and GB regions were quantified in R using *QuasR's* (version 1.22.10) *qCount* function. RPKM counts were calculated for the promoter and gene body count tables using the sum of the total reads on the promoter and gene body level as the library size for each sample. RPKMs were averaged per condition and log2-transformed with a pseudo-count of 0.1.

Quantifying mRNA (from Smart-seq2):

Counts on autosomal genes were quantified as described above. The counts per million (CPM) were quantified, averaged per condition, and log2-transformed with a pseudo-count of 1. The log-fold changes between *EedKO* and WT were calculated as the log2(*EedKO* CPM / WT CPM) for each gene. RPKM expression values of the autosomal genes were also calculated for the WT ESC condition, and averaged across replicates, to use in the definition of bipartite and bivalent genes. Bipartiteness and bivalency scores were calculated the same way as described above.

S5P logFC (Fig. 6a):

WT and *EedKO* counts for S5P and Nelf-b were quantified on the P, corrected for library size difference, and log2-transformed with a pseudo-count of 1. The logFC (*EedKO*/WT) violin plots of the ESCBip genes (top 100 bipartiteness scoring genes) were compared to the rest of the genes using the *vioplot* package[71] (version 0.3.0). The p-values were calculated using a two-sided Wilcoxon with the *wilcox.test* function from the *stats*[63] package in R with *alternative="two.sided"* and *paired = FALSE*.

Selecting genes positive for H3K27me3 on the gene body of ESC in WT:

We used the *Mclust* function from the *mclust* package[68] (verison 5.4.3) with *G=2* and *modelNames="V"* to fit a two-component Gaussian-mixture model on the gene body log2(RPKM+0.1) counts of the H3K27me3 WT mark, and used the fitted distributions to define a threshold value corresponding to an FDR of 0.05 as described in Minoux et al., 2019 [69]. Genes with H3K27me3 on the gene body higher than this threshold were selected as positive for the mark, and of those, genes that had a zero mRNA count in all samples were excluded (WT and *EedKO*), leaving us with a total of 3,457 genes that are positive for H3K27me3 on the gene body. These were further divided into 3 groups based on mRNA logFC between *EedKO* and WT: genes that

have a logFC < -1 (93), genes that have a logFC > 1 (1,067), and the remaining genes that have a -1 <= logFC <= 1 (2,297) (see Extended Data Fig. 7f).

S2P logFC (Extended Data Fig. 7f):

The S2P ChIP samples were quantified on the GB regions, corrected for library size differences, averaged per condition, and log2-transformed with a pseudo-count of 1. The logFC values were calculated by subtracting the WT log2-values from the *EedKO* log2-values, and displayed as violin plots for each of the 3 groups of genes (See Extended Data Fig. 7f). The p-values are the result of a two-sided Wilcoxon test using the *wilcox.test* function in R with *alternative="two.sided"* and *paired = FALSE*.

Sequence-specific characteristics of bipartite genes

Observed/expected CpG (oeCpG) ratio:

The regions 2kb upstream and 6kb downstream the TSS of the E14.5Bip and E14.5Biv genes were binned into consecutive 100bp bins, and the average oeCpG ratio was quantified in each set of genes. The oeCpG of a bin in a specific gene is calculated as the CG di-nucleotide frequency (with pseudo-count of 0.01) divided by the product of the C and G mono-nucleotide frequencies (with pseudo-count of 0.01) (See Extended Data Fig. 3f), using the *oligonucleotideFrequency* function from the *Biostrings*[72] package (version 2.50.2).

Motifs enriched in bipartite gene promoters:

The *monaLisa* package (version 0.1.28 and with R version 3.6.3, https://github.com/fmicompbio/monaLisa) was used to identify what motifs are enriched in E14.5Bip vs E14.5Biv promoters using the vertebrate list of motifs present in *JASPAR* (JASPAR2018)[73] and *Homer*[74] (version 4.10.4). Motifs that had an absolute log2-enrichment greater than 1 and were positively enriched in bipartite promoters were selected (RELB and FOXD1) (See Extended Data Fig. 3g).

Lavarone et al. Datasets (public):

mRNA MA plots

MA plots displaying logFC vs average logCPM values for each gene were made, using the public datasets from Lavarone et al[22]. A bipartiteness score was calculated using the same criteria as

described in previous sections, but using the ChIP-seq and mRNA-seq public datasets from Lavarone et al.[22] The top 100 bipartite genes specific to this dataset are highlighted in red in the MA plots (Extended Data Fig. 7h).

ATAC-seq and Ring1b (Fig. 6b,c):

The samples were quantified on the defined promoter and gene body regions, corrected for library size differences, and log2-transformed with a pseudo-count of 1. The top 100 bipartite genes of this ESC dataset are highlighted in red.

Public data sets used for analysis

A list of activity response genes (ARGs) (rapid primary response genes, delayed primary response genes and secondary response genes) from cultured cortical neurons treated by KCl were retrieved from Fig. 1 of Tyssowski et al., 2018[10]. ARGs from barrel cortex stimulated by environmental enrichment were retrived from Table 3 of Valles et al., 2011[11]. In Valles et al.,[11], 'early' ARGs (i.e. with a response comparable with IEGs) were defined as genes that are strongly up-regulated immediately after the completion of one hour of environmental enrichment (more than two folds) and show decreased expression after 4 hours (i.e. decreased expression at the time point of 4 hours compared with the time point of the completion of environmental enrichment). Eighteen genes were annotated in the mouse genome. 'Late' ARGs were defined as genes that are not strongly induced immediately after the completion of environmental enrichment, and show increased expression after 4 hours (at least 1.3 folds at the time point of 4 hours)[11]. Seven genes were annotated in the mouse genome. ARGs from visual cortex stimulated by light exposure were obtained from Table S3 of Hravatin et al., 2018[9]. 'Early' ARGs (i.e. with a response comparable with IEGs) were defined as genes that show increased expression in V1 excitatory neurons at the time point of 1 hour but not at the time point of 4 hours (at least three "a" and no "c" in excitatory neuron subpopulations). Twenty six genes were defined. 'Late'ARGs were defined as genes that are not induced at the time point of 1 hour but induced after 4 hours (at least two "c" and no "a" in excitatory neuron subpopulations). Nineteen genes were identified.

Public sequencing data sets were obtained as follows. Mouse cortical culture (GSE21161, GSE60192), mouse embryonic forebrain (GSE93011, GSE52386), mouse adult cortical excitatory neuron (GSE63137), mouse embryonic stem cells (GSE36114, GSE94250), mouse embryonic stem cells for PRC2-KO experiments in Lavarone et al., (GSE116603), mouse E14.5 heart tissues

(GSE82764, GSE82637, GSE82640, GSE78441, ENCSR068YGC), mouse E14.5 liver tissues (GSE78422, GSE82407, GSE82615, GSE82620, ENCSR032HKE) and E10.5 mouse neural crest cells isolated from the frontal nasal process (FNP) (GSE89437).

Supplementary Figures

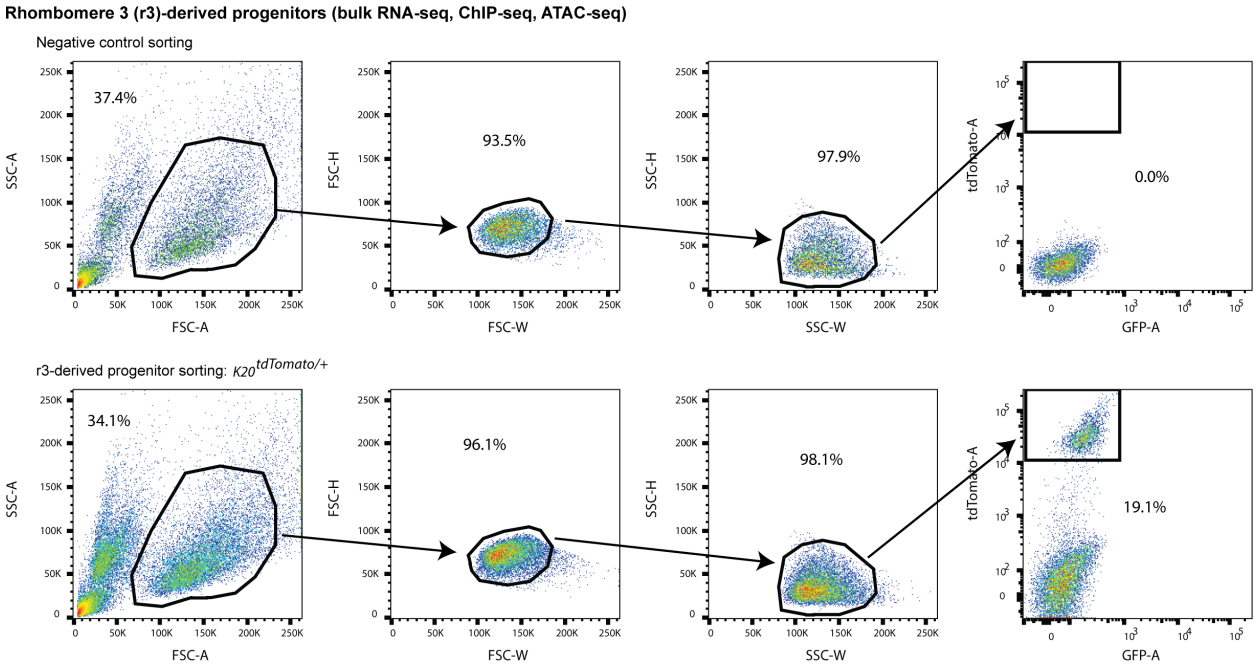

Supplementary Fig. 1 | FACS sequential gating strategy for E10.5 rhombomere 3 (r3)-derived progenitors.

Gating layouts of negative control and *K20*$^{tdTomato/+}$ mice are compared. Related to Fig. 1a, Extended Data Fig. 1. Nomenclatures for the mouse lines are summarized in Supplementary Table 1.

a **vPrV post-mitotic wild-type barrelette neurons (bulk RNA-seq, ChIP-seq, ATAC-seq)**

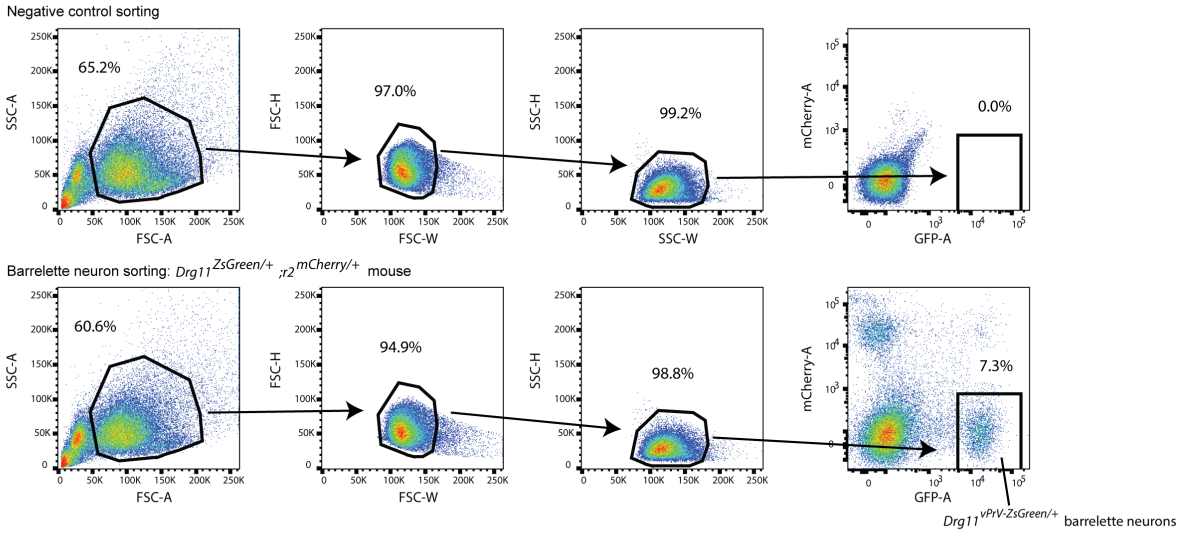

b **vPrV post-mitotic wild-type barrelette neurons (single-cell RNA-seq)**

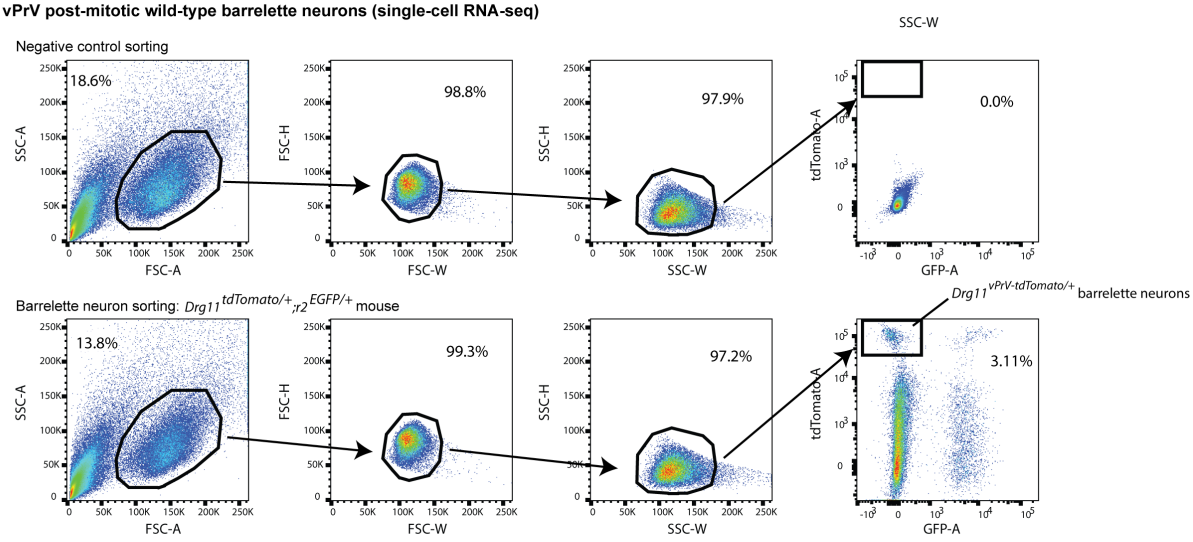

c **vPrV Kir2.1 over-expressing post-mitotic barrelette neurons**

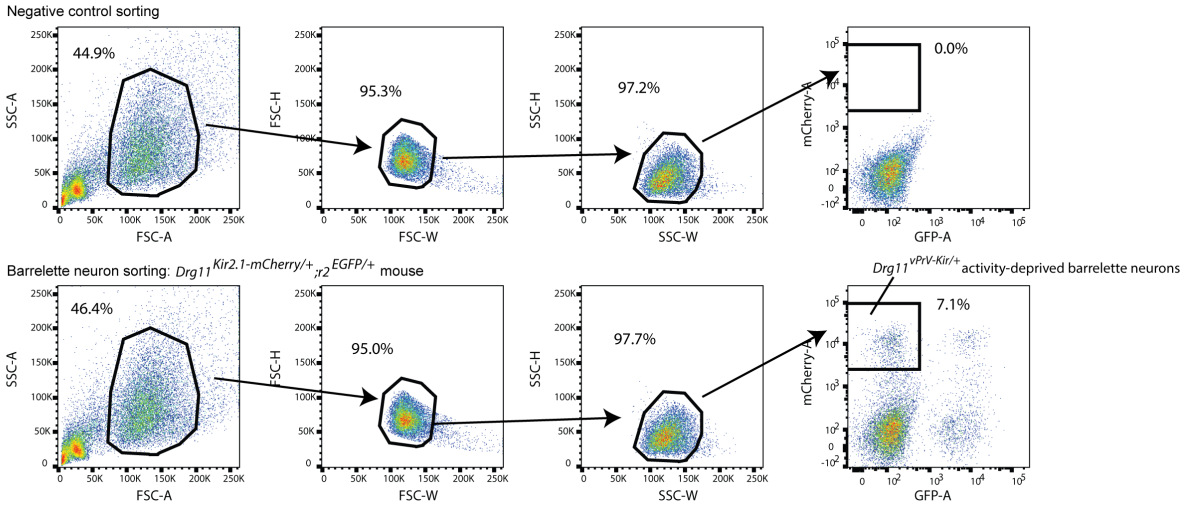

Supplementary Fig. 2 | FACS sequential gating strategy for vPrV post-mitotic barrelette neurons.

a, Gating layouts to sort wild-type *Drg11*$^{vPrV\text{-}ZsGreen/+}$ post-mitotic barrellette neurons. Negative control and *Drg11*$^{ZsGreen/+}$;*r2*$^{mCherry/+}$ mice are compared. Related to Fig. 1a, Extended Data Fig. 1a-c. **b**, Gating layouts to sort wild-type *Drg11*$^{vPrV\text{-}tdTomato/+}$ post-mitotic barrellette neurons. Negative control and *Drg11*$^{tdTomato/+}$;*r2*$^{EGFP/+}$ mice are compared. Related to Fig. 1a, Extended Data Fig. 1d. **c**, Gating layouts to sort neuronal activity-deprived Kir2.1 over-expressing *Drg11*$^{vPrV\text{-}Kir/+}$ post-mitotic barrellette neurons. Negative control and *Drg11*$^{Kir/+}$;*r2*$^{EGFP/+}$ mice are compared. Related to Fig. 1a, Extended Data Fig. 1e. Nomenclatures for the mouse lines and barrelette neurons are summarized in Supplementary Table 1.

a ***Ezh2cKO*** **r3-derived hindbrain cells (RNA-seq, ChIP-seq)**

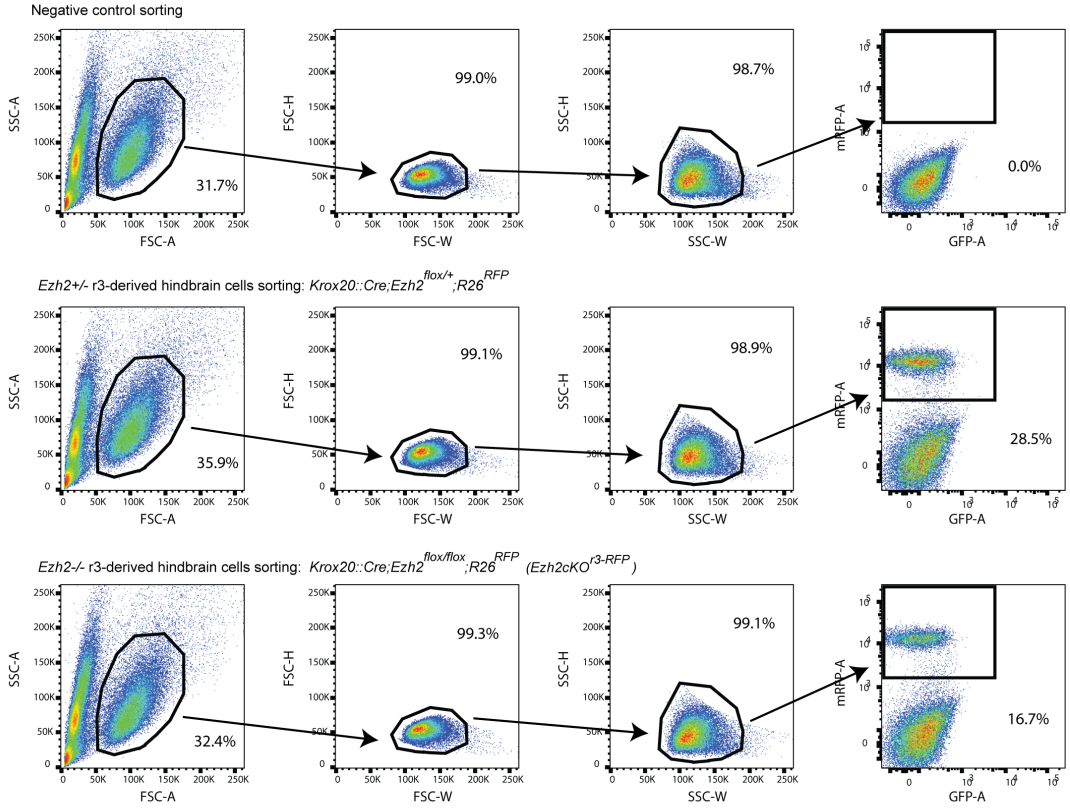

b ***Ezh2cKO*** **hindbrain cells (ATAC-seq, ChIP-seq)**

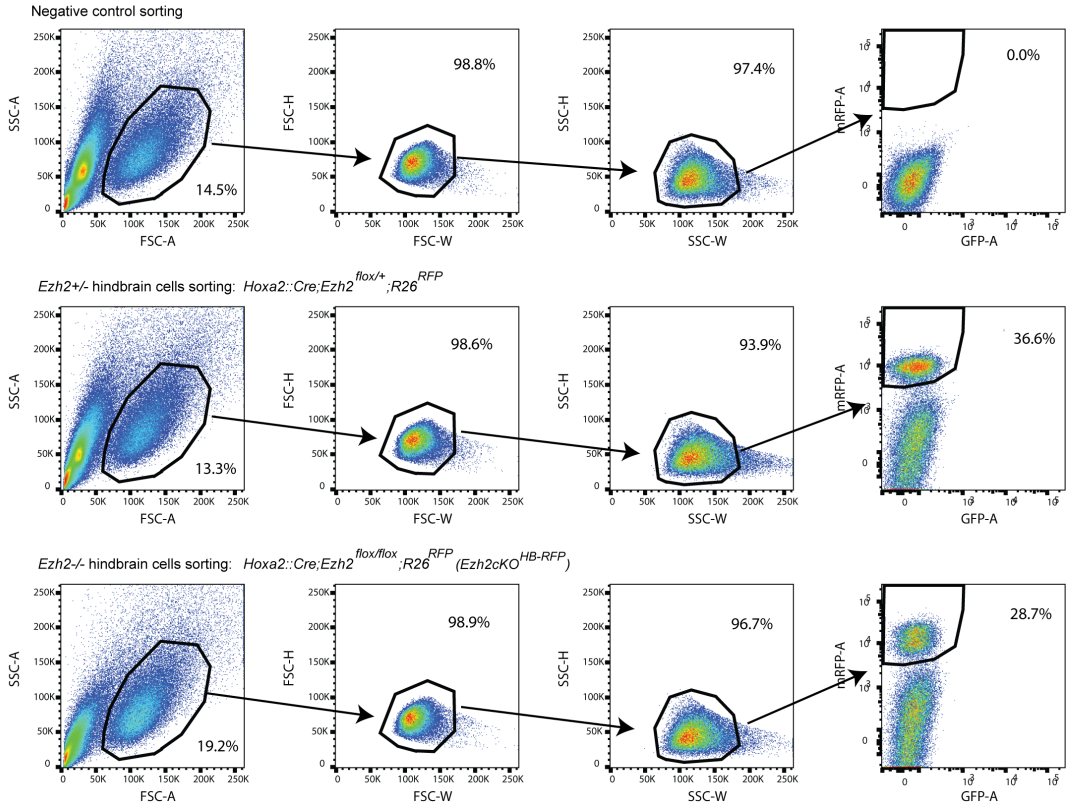

Supplementary Fig. 3 | FACS sequential gating strategy for E14.5 *Ezh2* conditionally knocked-out hindbrain cells.

a, Gating layouts to sort *Ezh2cKO* RFP-positive r3-derived hindbrain cells. Negative control, *Ezh2* heterozygous *Krox20::Cre;Ezh2*$^{flox/+}$*;R26*^{RFP} and *Ezh2* knocked-out *Krox20::Cre;Ezh2*$^{flox/flox}$*;R26*^{RFP} (*Ezh2cKO*$^{r3\text{-}RFP}$) mice are compared. Related to Fig. 5a-c, Extended Data Fig. 7c,d. **b**, Gating layouts to sort *Ezh2cKO* hindbrain cells. Negative control, *Ezh2* heterozygous *Hoxa2::Cre;Ezh2*$^{flox/+}$*;R26*^{RFP} and *Ezh2* knocked-out *Hoxa2::Cre;Ezh2*$^{flox/flox}$*;R26*^{RFP} (*Ezh2cKO*$^{HB\text{-}RFP}$) mice are compared. *Hoxa2::Cre* line, that labels from r2 to posterior hindbrain neurons, was utilized to collect relatively large number of hindbrain neurons to enable the molecular analysis of *Ezh2*-null neurons. Related to Fig. 5g, Extended Data Figs. 7e and 8i,j. Nomenclatures for the mouse lines are summarized in Supplementary Table 1.

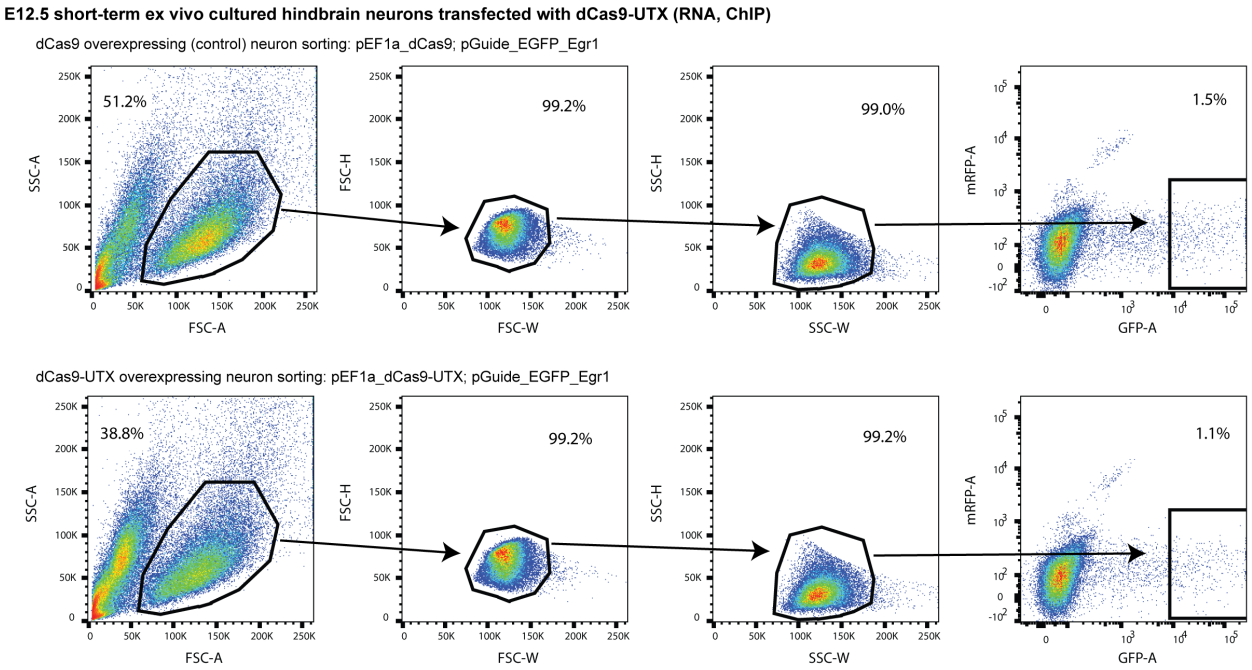

Supplementary Fig. 4 | FACS sequential gating strategy for E12.5 short-term ex vivo cultured hindbrain neurons overexpressing dCas9-Utx.

Representative gating layouts of dCas9 or dCas9-UTX overexpressing E12.5 short-term cultured hindbrain neurons. pGuide_EGFP_Egr1 plasmid which overexpresses EGFP and *Egr1* targeting guide RNA was co-transfected with pEF1a_dCas9 or pEF1a_dCas9-UTX plasmids, and EGFP-positive neurons were sorted. Related to Fig. 5d, Extended Data Fig. 8a-e.

Supplementary References

1 Oury, F. *et al.* Hoxa2- and rhombomere-dependent development of the mouse facial somatosensory map. *Science* **313**, 1408-1413, doi:10.1126/science.1130042 (2006).

2 Bechara, A. *et al.* Hoxa2 Selects Barrelette Neuron Identity and Connectivity in the Mouse Somatosensory Brainstem. *Cell Rep* **13**, 783-797, doi:10.1016/j.celrep.2015.09.031 (2015).

3 Moreno-Juan, V. *et al.* Prenatal thalamic waves regulate cortical area size prior to sensory processing. *Nat Commun* **8**, 14172, doi:10.1038/ncomms14172 (2017).

4 Li, Y., Erzurumlu, R. S., Chen, C., Jhaveri, S. & Tonegawa, S. Whisker-related neuronal patterns fail to develop in the trigeminal brainstem nuclei of NMDAR1 knockout mice. *Cell* **76**, 427-437 (1994).

5 Erzurumlu, R. S., Murakami, Y. & Rijli, F. M. Mapping the face in the somatosensory brainstem. *Nat Rev Neurosci* **11**, 252-263, doi:10.1038/nrn2804 (2010).

6 Kitazawa, T. & Rijli, F. M. Barrelette map formation in the prenatal mouse brainstem. *Curr Opin Neurobiol* **53**, 210-219, doi:10.1016/j.conb.2018.09.008 (2018).

7 Lo, F. S. & Erzurumlu, R. S. Neonatal sensory nerve injury-induced synaptic plasticity in the trigeminal principal sensory nucleus. *Exp Neurol* **275 Pt 2**, 245-252, doi:10.1016/j.expneurol.2015.04.022 (2016).

8 Erzurumlu, R. S. & Gaspar, P. Development and critical period plasticity of the barrel cortex. *Eur J Neurosci* **35**, 1540-1553, doi:10.1111/j.1460-9568.2012.08075.x (2012).

9 Hrvatin, S. *et al.* Single-cell analysis of experience-dependent transcriptomic states in the mouse visual cortex. *Nat Neurosci* **21**, 120-129, doi:10.1038/s41593-017-0029-5 (2018).

10 Tyssowski, K. M. *et al.* Different Neuronal Activity Patterns Induce Different Gene Expression Programs. *Neuron* **98**, 530-546 e511, doi:10.1016/j.neuron.2018.04.001 (2018).

11 Valles, A. *et al.* Genomewide analysis of rat barrel cortex reveals time- and layer-specific mRNA expression changes related to experience-dependent plasticity. *J Neurosci* **31**, 6140-6158, doi:10.1523/JNEUROSCI.6514-10.2011 (2011).

12 Joo, J. Y., Schaukowitch, K., Farbiak, L., Kilaru, G. & Kim, T. K. Stimulus-specific combinatorial functionality of neuronal c-fos enhancers. *Nat Neurosci* **19**, 75-83, doi:10.1038/nn.4170 (2016).

13 Kim, T. K. *et al.* Widespread transcription at neuronal activity-regulated enhancers. *Nature* **465**, 182-187, doi:10.1038/nature09033 (2010).

14 Malik, A. N. *et al.* Genome-wide identification and characterization of functional neuronal activity-dependent enhancers. *Nat Neurosci* **17**, 1330-1339, doi:10.1038/nn.3808 (2014).

15 West, A. E. & Greenberg, M. E. Neuronal activity-regulated gene transcription in synapse development and cognitive function. *Cold Spring Harb Perspect Biol* **3**, doi:10.1101/cshperspect.a005744 (2011).

16 Maze, I. *et al.* Critical Role of Histone Turnover in Neuronal Transcription and Plasticity. *Neuron* **87**, 77-94, doi:10.1016/j.neuron.2015.06.014 (2015).

17 Zaborowska, J., Egloff, S. & Murphy, S. The pol II CTD: new twists in the tail. *Nat Struct Mol Biol* **23**, 771-777, doi:10.1038/nsmb.3285 (2016).

18 Greer, C. B. *et al.* Histone Deacetylases Positively Regulate Transcription through the Elongation Machinery. *Cell Rep* **13**, 1444-1455, doi:10.1016/j.celrep.2015.10.013 (2015).

19 Jang, M. K. *et al.* The bromodomain protein Brd4 is a positive regulatory component of P-TEFb and stimulates RNA polymerase II-dependent transcription. *Mol Cell* **19**, 523-534, doi:10.1016/j.molcel.2005.06.027 (2005).

20 Stroud, H. *et al.* An Activity-Mediated Transition in Transcription in Early Postnatal Neurons. *Neuron* **107**, 874-890 e878, doi:10.1016/j.neuron.2020.06.008 (2020).

21 Schoeftner, S. *et al.* Recruitment of PRC1 function at the initiation of X inactivation independent of PRC2 and silencing. *EMBO J* **25**, 3110-3122, doi:10.1038/sj.emboj.7601187 (2006).

22 Lavarone, E., Barbieri, C. M. & Pasini, D. Dissecting the role of H3K27 acetylation and methylation in PRC2 mediated control of cellular identity. *Nat Commun* **10**, 1679, doi:10.1038/s41467-019-09624-w (2019).

23 Chen, F. X., Smith, E. R. & Shilatifard, A. Born to run: control of transcription elongation by RNA polymerase II. *Nat Rev Mol Cell Biol* **19**, 464-478, doi:10.1038/s41580-018-0010-5 (2018).

24 Schaukowitch, K. *et al.* Enhancer RNA facilitates NELF release from immediate early genes. *Mol Cell* **56**, 29-42, doi:10.1016/j.molcel.2014.08.023 (2014).

25 Muse, G. W. *et al.* RNA polymerase is poised for activation across the genome. *Nat Genet* **39**, 1507-1511, doi:10.1038/ng.2007.21 (2007).

26 Saha, R. N. *et al.* Rapid activity-induced transcription of Arc and other IEGs relies on poised RNA polymerase II. *Nat Neurosci* **14**, 848-856, doi:10.1038/nn.2839 (2011).

27 Schuettengruber, B., Bourbon, H. M., Di Croce, L. & Cavalli, G. Genome Regulation by Polycomb and Trithorax: 70 Years and Counting. *Cell* **171**, 34-57, doi:10.1016/j.cell.2017.08.002 (2017).

28 Simon, J. A. & Kingston, R. E. Mechanisms of polycomb gene silencing: knowns and unknowns. *Nat Rev Mol Cell Biol* **10**, 697-708, doi:10.1038/nrm2763 (2009).

29 Schlumm, F., Mauceri, D., Freitag, H. E. & Bading, H. Nuclear calcium signaling regulates nuclear export of a subset of class IIa histone deacetylases following synaptic activity. *J Biol Chem* **288**, 8074-8084, doi:10.1074/jbc.M112.432773 (2013).

30 Sagner, A. & Briscoe, J. Morphogen interpretation: concentration, time, competence, and signaling dynamics. *Wiley Interdiscip Rev Dev Biol* **6**, doi:10.1002/wdev.271 (2017).

31 Mayer, A., Landry, H. M. & Churchman, L. S. Pause & go: from the discovery of RNA polymerase pausing to its functional implications. *Curr Opin Cell Biol* **46**, 72-80, doi:10.1016/j.ceb.2017.03.002 (2017).

32 Min, I. M. *et al.* Regulating RNA polymerase pausing and transcription elongation in embryonic stem cells. *Genes Dev* **25**, 742-754, doi:10.1101/gad.2005511 (2011).

33 Stroud, H. *et al.* Early-Life Gene Expression in Neurons Modulates Lasting Epigenetic States. *Cell* **171**, 1151-1164 e1116, doi:10.1016/j.cell.2017.09.047 (2017).

34 Baker, S. A. *et al.* An AT-hook domain in MeCP2 determines the clinical course of Rett syndrome and related disorders. *Cell* **152**, 984-996, doi:10.1016/j.cell.2013.01.038 (2013).

35 Frasch, M., Chen, X. & Lufkin, T. Evolutionary-conserved enhancers direct region-specific expression of the murine Hoxa-1 and Hoxa-2 loci in both mice and Drosophila. *Development* **121**, 957-974 (1995).

36 Schmidl, C., Rendeiro, A. F., Sheffield, N. C. & Bock, C. ChIPmentation: fast, robust, low-input ChIP-seq for histones and transcription factors. *Nat Methods* **12**, 963-965, doi:10.1038/nmeth.3542 (2015).

37 Picelli, S. *et al.* Full-length RNA-seq from single cells using Smart-seq2. *Nat Protoc* **9**, 171-181, doi:10.1038/nprot.2014.006 (2014).

38 Splinter, E., de Wit, E., van de Werken, H. J., Klous, P. & de Laat, W. Determining long-range chromatin interactions for selected genomic sites using 4C-seq technology: from fixation to computation. *Methods* **58**, 221-230, doi:10.1016/j.ymeth.2012.04.009 (2012).

39 Nagano, T. *et al.* Single-cell Hi-C for genome-wide detection of chromatin interactions that occur simultaneously in a single cell. *Nat Protoc* **10**, 1986-2003, doi:10.1038/nprot.2015.127 (2015).

40 Yost, K. E., Carter, A. C., Xu, J., Litzenburger, U. & Chang, H. Y. ATAC Primer Tool for targeted analysis of accessible chromatin. *Nat Methods* **15**, 304-305, doi:10.1038/nmeth.4663 (2018).

41 Konermann, S. *et al.* Genome-scale transcriptional activation by an engineered CRISPR-Cas9 complex. *Nature* **517**, 583-588, doi:10.1038/nature14136 (2015).

42 Cong, L. *et al.* Multiplex genome engineering using CRISPR/Cas systems. *Science* **339**, 819-823, doi:10.1126/science.1231143 (2013).

43 Osakada, F. & Callaway, E. M. Design and generation of recombinant rabies virus vectors. *Nat Protoc* **8**, 1583-1601, doi:10.1038/nprot.2013.094 (2013).

44 Gaidatzis, D., Lerch, A., Hahne, F. & Stadler, M. B. QuasR: quantification and annotation of short reads in R. *Bioinformatics* **31**, 1130-1132, doi:10.1093/bioinformatics/btu781 (2015).

45 Zhang, Y. *et al.* Model-based analysis of ChIP-Seq (MACS). *Genome Biol* **9**, R137, doi:10.1186/gb-2008-9-9-r137 (2008).

46 Frankish, A. *et al.* GENCODE reference annotation for the human and mouse genomes. *Nucleic Acids Res* **47**, D766-D773, doi:10.1093/nar/gky955 (2019).

47 Patro, R., Duggal, G., Love, M. I., Irizarry, R. A. & Kingsford, C. Salmon provides fast and bias-aware quantification of transcript expression. *Nat Methods* **14**, 417-419, doi:10.1038/nmeth.4197 (2017).

48 Dobin, A. *et al.* STAR: ultrafast universal RNA-seq aligner. *Bioinformatics* **29**, 15-21, doi:10.1093/bioinformatics/bts635 (2013).

49 Li, H. *et al.* The Sequence Alignment/Map format and SAMtools. *Bioinformatics* **25**, 2078-2079, doi:10.1093/bioinformatics/btp352 (2009).

50 Martin, M. Cutadapt removesadapter sequences from high-throughput sequencing reads. EMBnet.journal 17.1.

51 Langmead, B. & Salzberg, S. L. Fast gapped-read alignment with Bowtie 2. *Nat Methods* **9**, 357-359, doi:10.1038/nmeth.1923 (2012).

52 Langmead, B., Trapnell, C., Pop, M. & Salzberg, S. L. Ultrafast and memory-efficient alignment of short DNA sequences to the human genome. *Genome Biol* **10**, R25, doi:10.1186/gb-2009-10-3-r25 (2009).

53 van de Werken, H. J. *et al.* 4C technology: protocols and data analysis. *Methods Enzymol* **513**, 89-112, doi:10.1016/B978-0-12-391938-0.00004-5 (2012).

54 Lawrence, M., Gentleman, R. & Carey, V. rtracklayer: an R package for interfacing with genome browsers. *Bioinformatics* **25**, 1841-1842, doi:10.1093/bioinformatics/btp328 (2009).

55 Ritchie, M. E. *et al.* limma powers differential expression analyses for RNA-sequencing and microarray studies. *Nucleic Acids Res* **43**, e47, doi:10.1093/nar/gkv007 (2015).

56 Alasoo, K. Wiggleplotr: Make read coverage plots from bigwig files. (2019).

57 Soneson, C., Love, MI. & Robinson, MD. Differential analyses for RNA-seq: transcript-level estimates improve gene-level inferences [version 2; peer review: 2 approved] F1000Research **4**, 1521 (2016).

58 Zheng, G. X. *et al.* Massively parallel digital transcriptional profiling of single cells. *Nat Commun* **8**, 14049, doi:10.1038/ncomms14049 (2017).

59 Lun, A. T. L. *et al.* EmptyDrops: distinguishing cells from empty droplets in droplet-based single-cell RNA sequencing data. *Genome Biol* **20**, 63, doi:10.1186/s13059-019-1662-y (2019).

60 McCarthy, D. J., Campbell, K. R., Lun, A. T. & Wills, Q. F. Scater: pre-processing, quality control, normalization and visualization of single-cell RNA-seq data in R. *Bioinformatics* **33**, 1179-1186, doi:10.1093/bioinformatics/btw777 (2017).

61 Lun, A. T., McCarthy, D. J. & Marioni, J. C. A step-by-step workflow for low-level analysis of single-cell RNA-seq data with Bioconductor. *F1000Res* **5**, 2122, doi:10.12688/f1000research.9501.2 (2016).

62 Maaten, L.J.P.V.D. & Hinton, GE. Visualizing High-Dimensional Data using t-SNE. Journal of Machine Learning Research **9**, 2579-2605 (2008).

63 R Core Team. R: A language and environment for statistical computing. (R Foundation for Statistical Computing, VA, 2020).

64 Gehlenborg, N. UpSetR: A More Scalable Alternative to Venn and Euler Diagrams for Vi sualizing Intersecting Sets. R package version 1.4.0. https://CRAN.R-project.org/package =UpSetR (2019).

65 Venables, W.N. & Ripley, B.D. Modern Applied Statistics with S. (Fourth Edition. Springer, NY, 2002).

66 Durinck, S., Spellman, P. T., Birney, E. & Huber, W. Mapping identifiers for the integration of genomic datasets with the R/Bioconductor package biomaRt. *Nat Protoc* **4**, 1184-1191, doi:10.1038/nprot.2009.97 (2009).

67 Robinson, M. D., McCarthy, D. J. & Smyth, G. K. edgeR: a Bioconductor package for differential expression analysis of digital gene expression data. *Bioinformatics* **26**, 139-140, doi:10.1093/bioinformatics/btp616 (2010).

68 Scrucca, L., Fop, M., Murphy, T. B. & Raftery, A. E. mclust 5: Clustering, Classification and Density Estimation Using Gaussian Finite Mixture Models. *R J* **8**, 289-317 (2016).

69 Minoux, M. *et al.* Gene bivalency at Polycomb domains regulates cranial neural crest positional identity. *Science* **355**, doi:10.1126/science.aal2913 (2017).

70 O'Connell, J. & Hojsgaard, S. Hidden Semi Markov Models for Multiple Observation Sequences: The mhsmm Package for R. Journal of Statistical Software **39**, 4 (2011).

71 Adler, D. & S. Kelly, S. K. vioplot: violin plot. R package version 0.3.4 https://github.co m/TomKellyGenetics/vioplot (2019).

72 Pagès, H., Aboyoun, P., Gentleman, R. & DebRoy, S. Biostrings: Efficient manipulation of biological strings. R package version 2.56.0. (2020).

73 Tan, Ge. JASPAR2018: Data package for JASPAR 2018. R package version 1.1.1. http://jaspar.genereg.net/ (2017).

74 Heinz, S. *et al.* Simple combinations of lineage-determining transcription factors prime cis-regulatory elements required for macrophage and B cell identities. *Mol Cell* **38**, 576-589, doi:10.1016/j.molcel.2010.05.004 (2010).